ACS OMEGA

Open Access

http://pubs.acs.org/journal/acsodf

Article

Elucidating the Advancement in the Optoelectronics Characteristics of Benzoselenadiazole-Based A2-D-A1-D-A2-Type Nonfullerene Acceptors for Efficient Organic Solar Cells

Hira Naz,[⊥] Muhammad Adnan,[⊥] Zobia Irshad, Riaz Hussain,* Hany W. Darwish, and Mahmood Ahmed

Cite This: *ACS Omega* 2024, 9, 44668−44688

Read Online

ACCESS | Metrics & More | Article Recommendations | Supporting Information

ABSTRACT: The potential applications of nonfullerene acceptors (NFAs) such as tunable band gaps, improved charge separation, wide-range absorption, enhanced power conversion efficiency, and operational stability make them highly favorable for organic photovoltaic applications. Herein, we designed eight novel structurally modified nonfused benzoselenadiazole (BSe)-based A2-D-A1-D-A2-type NFAs for efficient organic solar cells (OSCs). These newly modeled BSe-based NFA series contain BSe as the central core. We employed strong electron-withdrawing moieties at terminal acceptor A2 to further enhance the optical, optoelectronics, and photovoltaic characteristics of OSCs. These designed molecules (HNM1−HNM8) along with the synthetic reference molecule (HNM) were thoroughly characterized by using efficient and advanced quantum chemical simulation approaches. Thus, to ascertain the enhancement of both optical and photochemical response, a thorough density functional theory (DFT) study was carried out using the M062X level in association with the 6-31G(d,p) basis set. All of the investigated molecules (HNM1−HNM8) had their excited states calculated using the time-dependent density functional theory method. The newly designed molecules (HNM1−HNM8) presented narrower band gaps, improved absorption and optoelectronics properties, and reduced excitation and binding energies. The electrostatic potential, density of states, transition density matrix, ionization potential, and electron affinity analysis of this newly designed (HNM1−HNM8) series revealed a strong coherence with those of the reference HNM molecule. Electron density difference mapping allowed us to visualize the spatial movement of electrons between the donor and acceptor molecules during excitation. This insight helps us to understand the efficiency of charge separation and recombination processes that are critical for the performance of organic photovoltaics. The reorganization energy and charge transfer analysis suggests that HNM1−HNM8 molecules could act as NFAs for organic photovoltaic applications to enhance their efficiency further. The donor: acceptor charge transfer analysis was also carried out, which revealed that the PTB7-Th:HNM2 donor:acceptor complex shows a great charge transportation process at the donor−acceptor interface. Moreover, the photovoltaic analysis shows that the designed (HNM1−HNM8) NFA series has a great potential to produce improved open-circuit voltage and fill factor values, which may be helpful in enhancing the overall PCEs of the OSCs.

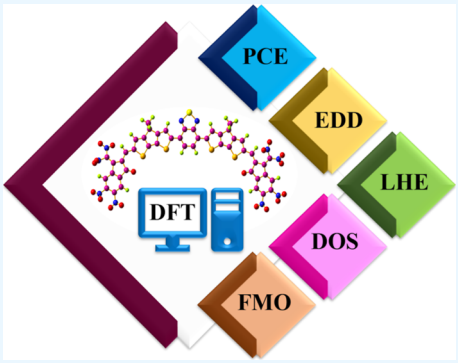

1. INTRODUCTION

Fullerene derivatives have been utilized as acceptors in bulk heterojunction (BHJ) active layers to fabricate organic solar cells (OSCs) for a considerable amount of time because of their high electron mobility and suitable electron affinity (EA) for electron transfer from the donor polymer. The power conversion efficiency (PCE) of these OSCs has been reported to be 10−11%.[1,2] It is challenging to modify the current density (J_{sc}) and open-circuit voltages (V_{oc}) of OSCs due to the poor absorption of these materials in the visible region, which results in significant energy loss.[3] Nonfullerene small molecule acceptors (NFSMAs), in contrast to fullerene derivatives, offer a wide range of structural variety, which makes it easier to tune their optical characteristics and orbitals of Frontier molecules.[4] NFSMAs are conjugated skeletons that, in general, include electron-donating (D) and electron-accepting (A) units to produce A-DA′D-A[5] or A-D-A associations. The chemical alteration of the A,[6] D,[7] and A′[8] units and side chains of the conjugated backbones can readily modify the highest occupied molecular orbitals (HOMOs)/lowest unoccupied molecular orbitals (LUMOs) and the optimal absorption profile of NFSMAs as well as the morphology of the active layer blended film. Right now, Y6 and its derivatives are the most effective NFSMAs. They have an A-DA′D-A configuration with benzothiadiazole (BT) and

Received: August 13, 2024
Revised: October 8, 2024
Accepted: October 11, 2024
Published: October 22, 2024

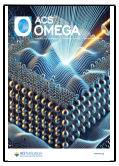

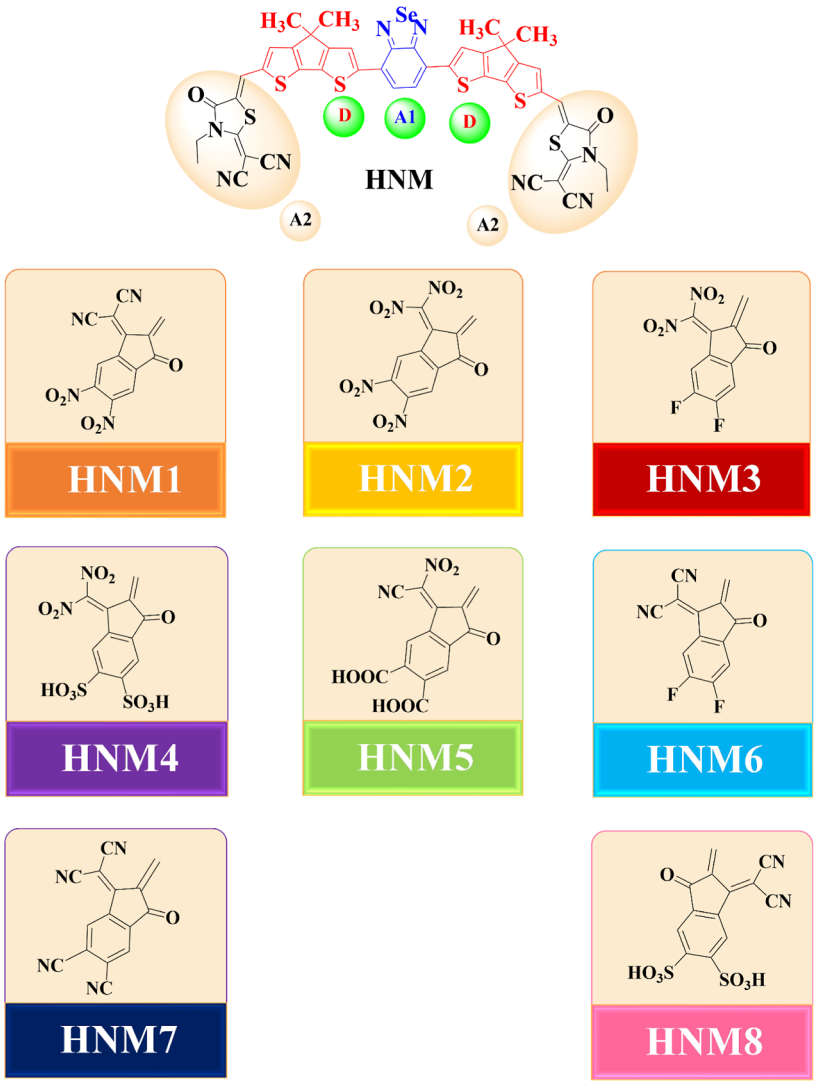

Figure 1. Molecular structures of the used functional end-capped moieties to modify the synthetic reference HNM to design a new HNM1−HNM8 NFA series.

thieno[3,2*b*]thiophene[5,9] as the central fused-ring core. OSCs constructed with Y-type NFSMAs have been able to attain efficiencies of more than 18% owing to the employment of various molecular designs, device interface engineering, and BHJ active layer morphological improvement.[8,10] Although OSCs based on FR-NFSMAs have outstanding PCE values, synthesis of these acceptors' massive fused backbones is a multistep process that generates low yields during purification by crystallization of the central core units. The commercial application of FR-NFSMAs in OSCs is restricted by these drawbacks.[11] Thus, one area of interest is the construction of nonfused-ring (NFR) nonfullerene acceptors (NFAs) with an A-D-A′(D′)-D-A arrangement.[12]

To create tricyclic or more simple aromatic compounds, the NFR approach entails modifying the fused cores such as the DA′D units in the Y-series materials. Usually, the goal of developing NFR-based NFSMAs is to lower the overall cost by increasing the efficiency of the synthetic route or reducing the synthesis's difficulty. The literature has published numerous examples of NFR-NFSMA systems with PCE values over 15%[13,14] and outstanding stability.[13,15]

The choice of the A′ unit is critical in the NFR-NFSMA system design because it affects the molecular packing behavior, intramolecular interactions, light harvesting, and energy levels inside the system. Compared with their FR-NFSMA counterparts, the PCE values of OSCs based on these acceptors are still significantly lower. BT derivatives currently make up the majority of the A′ units employed in NFSMAs. Benzoselenadiazole (BSe) is an interesting addition to BT because it substitutes a selenium (Se) atom for a sulfur (S) atom. Se is less electronegative than S and is larger than S, so the organic semiconductors containing Se should absorb more light in the near-infrared portion of the solar spectrum. Furthermore, compared to S analogues, Se-containing units ought to be more polarizable because of their larger dipole moment. The charge transport in the BHJ film may be enhanced by the Se···Se interaction through better intermolecular interactions with the polymer donor.[16]

Li and colleagues created Y6Se, a Y6 derivative with an electron-deficient fused core containing BSe.[17] Asymmetric NFAs, or BTPSe, were recently created by Hai et al. using a fused BSe electron-deficient core in a DA′D system. A greater PCE value of 14.20% was obtained by the resulting PBDB-

https://doi.org/10.1021/acsomega.4c07436
ACS Omega 2024, 9, 44668−44688

T:BTPSe OSCs than by a BT core.[18] An efficiency of 18.05% was provided by the OSC based on PM6:m-Ph4F-Ts. Zhang et al. created two isomeric alkylphenyl-substituted selenophene-[3,2-*b*]thiophene-based NF-SMAs with different substitution sites. These are known as m-Ph4F-TS and m-Ph4F-ST.[19] Before the pioneering work by Casanova et al.,[20] there had been no reports of NFR NFSMAs incorporating BSe units.

Because of their favorable characteristics, such as their reduced π^*-orbital and robust electron-donating ability, cyclopentadithiophene (CPDT) and its derivatives rank among the most important donor units among the promising range of electron-donor units.[21,22] Because of their elevated LUMO energy levels, rhodanine-based NFAs have higher V_{OC} values. Furthermore, it is simple to adjust the optical and electrochemical characteristics of rhodamine-based monomers by modifying their structure. Selenium was added to the central core of the newly created NFSMA by Casanova et al. to create a new acceptor−donor-core acceptor−donor−acceptor (A2-D-A1-D-A2) NFSMA, NC2.[20] These compounds have rhodamine dicyanomethylene moieties (RdCN) as the terminal acceptors (A2), CPDT as the donor (D), and BSe as the core acceptor (A1). This end-capped-acceptor A2 molecule is a useful tool for producing efficient OSCs by modifying end-capped moieties.

In this work, eight new BSe-based A2-D-A1-D-A2-type nonfused NFAs (HNM1−HNM8) have been designed using efficient electron-withdrawing functional units on the synthetic HNM (NC2) molecule. With these alternative electron-withdrawing groups, there is a great deal of potential for enhancing the charge separation between the donor and acceptor components as well as getting the narrower energy gaps and expanding the absorption ranges compared to the synthetic HNM molecule. The optical and photovoltaic properties of these materials (HNM1−HNM8) were then characterized theoretically by using various advanced density functional theory (DFT) and time-dependent density functional theory (TD-DFT)) techniques. Remarkably, the developed materials (HNM1−HNM8) exhibit comparable V_{oc} and FF values, contributing to the devices' enhanced photovoltaic performance. Figure 1 depicts the chemically altered end-capped acceptor A2 moieties used to design the HNM1−HNM8 NFAs series from the synthetic reference HNM molecule. Our research sheds insight on the structure−property relationship of NFRs with A2-D-A1-D-A2-type NFAs based on the BSe-based core and provides a novel way for developing highly efficient nonfused NFAs for OSCs.

2. COMPUTATIONAL DETAILS

In the scientific world, DFT is a very useful computing tool. It has been shown that this technique can be used to reliably and precisely assess a large range of quantum mechanical properties.[23] All computational investigations were conducted using the Gaussian 09[24] program. We designed the computationally processable shape of the reference molecule using GaussView 6.0.[25]

Initially, five different DFT-based functionals, including B3LYP,[26] MPW1PW91,[27] CAM-B3LYP,[28] ωB97XD,[29] and M062X[30] at 6-31G(d,p), were used to optimize the HNM (reference molecule). The chosen functionals were then used to conduct additional research. DFT was conducted at the functional levels stated above in both the gaseous phase and solvent (dichloromethane) to estimate the absorption maxima (λ_{max}) of the standard reference molecule. The ideal functional level for this experiment was found by comparing the theoretically expected UV−vis value of the HNM at these levels to the observed UV−vis range using a moderately common technique. It is generally accepted as the most acceptable theoretical functional; we found that the UV−vis λ_{max} of the HNM molecule, measured at 6-31G(d,p)/M062X, was the one that matched the actual absorption maximum value the closest. Therefore, utilizing this functional level (i.e., M062X), the fundamental optical and photovoltaic characteristics of HNM1-HNM8 were calculated.

We performed charge transfer analysis at the selected DFT level, open circuit voltage, FMO, geometric optimization, electron density difference (EDD), molecular electrostatic potential, NPA, density of state (DOS), ionization potential (IP), EA, TDM, maximal absorption (λ_{max}), and reorganization energy (RE) (λ_e and λ_h) for acceptors HNM[20] and HNM1−HNM8. An absorption spectrum with an origin of 8.0.[31] was created using data from a Gaussian assessment. PyMOlyze-1.1[32] and Origin 8.0 were used to study the DOS of the HNM and HNM1−HNM8 molecules to evaluate the electronegativity of individual and group atoms within electronic mass states that could exist. Using Multiwfn software,[33] TDM data were transformed into maps illustrating the atoms' interactions and mobility during excitation.

The most important factor in determining a molecule's electron and hole mobilities is its RE. The RE is further divided into two categories: (i) external and (ii) internal RE. The first is connected to changes in the external environment of the molecule and is the often-underappreciated effect of polarity on charge transport, whereas the second is related to the adjustments made to the internal geometry of the molecule. Equations 1 and 2 were used to estimate the REs (λ_e and λ_h).[34]

$$\lambda_e = [E_0^- - E_-] + [E_-^0 - E_0] \quad (1)$$

$$\lambda_h = [E_0^+ - E_+] + [E_+^0 - E_0] \quad (2)$$

Here, optimized anionic and cationic molecules are used to calculate the respective anionic and cationic energies, E_- and E_+. The optimized neutral molecule's ground state energy is denoted by E_0, while the anion and cation energies, calculated from the molecular geometry of the cationic and anionic structures in the neutral condition, are represented by E_0^+ and E_0^-, respectively. Additionally, the energy of the neutral molecule is represented by E_+^0 and E_-^0, which are the results of the optimized cationic and anionic geometry.

3. RESULTS AND DISCUSSION

This study aimed to theoretically design a novel acceptor molecule based on BSe, incorporating potential acceptor moieties and evaluating their expected optical properties. The experimentally synthesized acceptor−donor-core acceptor−donor−acceptor (A2-D-A1-D-A2) based on BSe was used as the reference HNM(20) in this inquiry. The rhodamine dicyanomethylene acceptor (A2) moiety, BSe as the core acceptor (A1), and CPDT as the donor unit (D) are the constituents that make up the reference HNM structure (Figure 1). The molecular structures of the synthetic reference HNM and designed HNM1−HNM8 molecules are shown in Figure S1, and their optimized geometries are shown in Figure S2. It is essential to screen the pendant acceptor group to produce high-quality photovoltaic capabilities. To create new materials with exceptional photovoltaic properties, HNM's structural tailoring was carried out; as a result, the donor

https://doi.org/10.1021/acsomega.4c07436
ACS Omega 2024, 9, 44668−44688

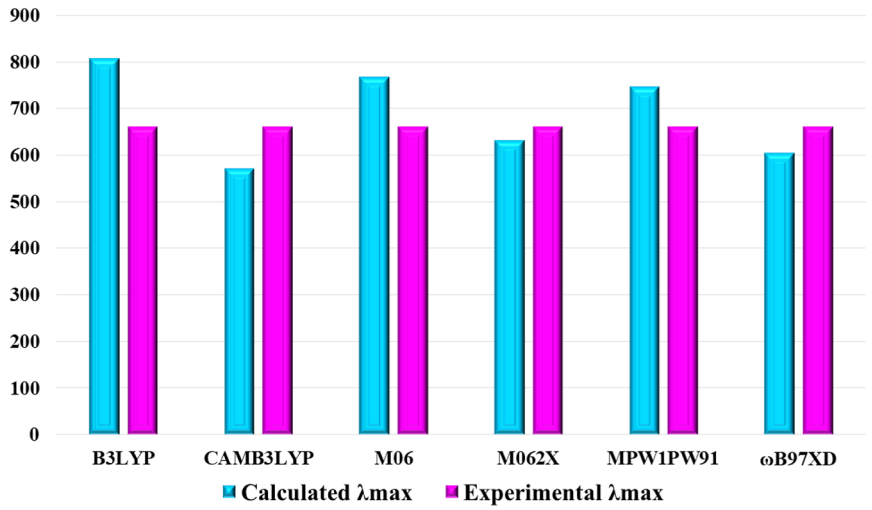

Figure 2. Comparison of the experimental and theoretical UV−visible values of the synthetic reference HNM in dichloromethane solvent using various DFT functionals.

component of HNM remained unaltered, and alternative acceptor units were substituted for the end-capped moiety A2, as illustrated in Figure 1. By creating acceptor moiety A2 of HNM with distinct end-capped groups, eight newly built molecules, named HNM1, HNM2, HNM3, HNM4, HNM5, HNM6, HNM7, and HNM8, were customized.

To choose the optimal DFT functional with UV values that are significantly closer to or comparable to the experimental UV value of the reference molecule (HNM), we first optimized the HNM molecule by using a variety of DFT functionals. In the gas and solvent phases of our optimization, we used B3LYP, CAM-B3LYP, MPW1PW91, ωB97XD, M06, and M062X at 6-31G(d,p). Figure 2 shows that among all the DFT functionals M06 (766.23 nm),[35] M062X (631.80 nm), MPW1PW91 (746.80 nm), CAM-B3LYP (570.51 nm), ωB97XD (604.39 nm), and B3LYP (806.24 nm), the HNM molecule exhibited a highly red-shifted absorption phenomenon and presented an excellent value of UV−visible absorption. Compared to the other functionals used, its UV-value is closer to M062X, so we chose M062X and 6-31G(d,p) for further characterization of the developed molecules HNM1−HNM8 and HNM after this optimization. As demonstrated in Figure 2, the UV-value of HNM obtained experimentally is 660.00 nm, but the value achieved using M062X at 6-31G(d,p) is 631.80 nm, which is considerably closer and comparable. Figure 3 optimized dihedral angles of the designed molecules that we optimized at the ground state after choosing the DFT functional.

3.1. Dihedral Angle Analysis. A glimpse of the degree of optimization and the conjugation of the molecule is provided by the dihedral angle. The molecules with three-dimensional geometry are represented by higher values of the dihedral angles having minimal planarity.[36] True structural planarity, which promotes self-aggregation and aids in charge transfer by conjugation, will result from smaller dihedral angle values. The dihedral angles on the left and right sides of the donor and terminal acceptor are denoted by Φ1 and Φ2, respectively. Figure 3 illustrates the dihedral angle values on both sides of the reference molecule HNM, which further explains the planar geometry of the molecule. These values are −0.27 and −0.27°. Table 1 makes it evident that there are significant parallels between the dihedral angle values on the two

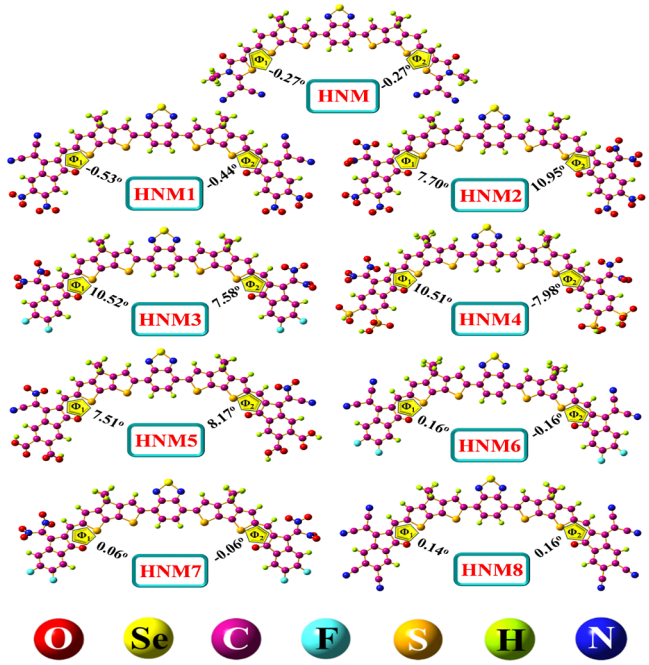

Figure 3. Optimized structures along with the calculated dihedral angle of the synthetic reference HNM and designed HNM1−HNM8 molecules.

Table 1. Calculated Dihedral Angles of the Optimized Synthetic Reference HNM and Designed HNM1−HNM8 Molecules

molecules	Φ_1	Φ_2
HNM	−0.27	−0.27
HNM1	−0.53	−0.44
HNM2	7.70	10.95
HNM3	10.52	7.58
HNM4	10.51	−7.98
HNM5	7.51	8.17
HNM6	0.16	−0.16
HNM7	0.06	−0.06
HNM8	0.14	0.16

https://doi.org/10.1021/acsomega.4c07436
ACS Omega 2024, 9, 44668−44688

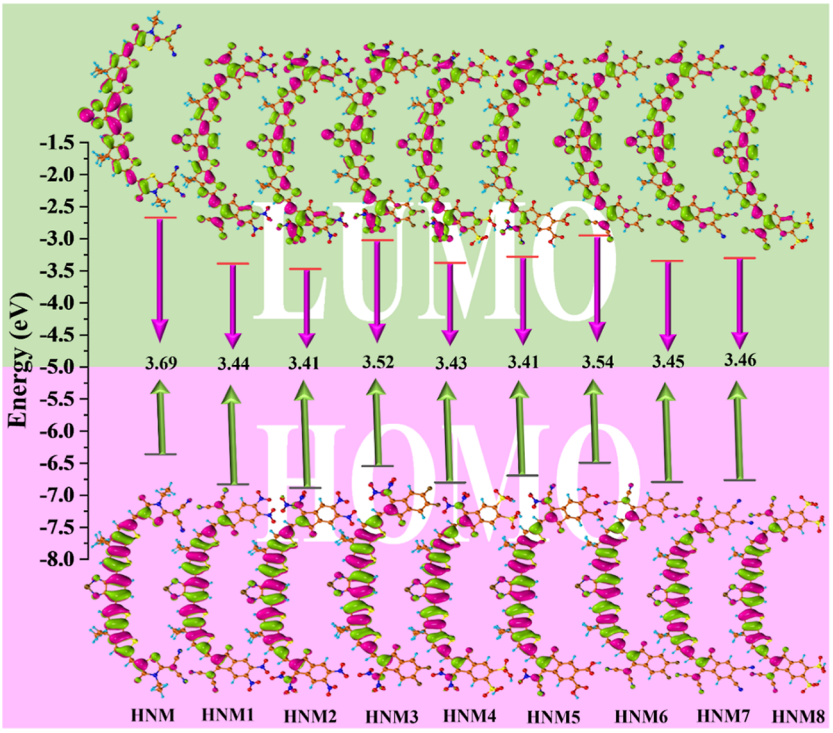

Figure 4. Frontier molecular orbitals distribution of the synthetic reference HNM and designed HNM1−HNM8 molecules.

computed sites for every molecule under study (HNM1−HNM8), which explains their planner structure. Every molecule's dihedral angle falls between −0.06° and 10.95°. Since bulky terminal acceptor groups can cause steric hindrance, all molecules have dihedral angle values that have a significant contribution to the determination of charge transport capacities and elaborate their minute divergence from planarity.

3.2. Frontier Molecular Orbital Analysis. An overview of the likelihood of charge transfer from the ground state to the excited state in OSCs is provided by the examination of the HOMO and LUMO. Using FMOs, one may qualitatively assess the orbitals' bonding characteristics, which control the electronic transitional changes for every pair of bonded atoms. OSC causes the electrons to migrate from a lower-energy ground state to a higher-energy excited state by absorbing photons from sunlight. This results in electronic transitions from the HOMO orbital to the LUMO orbital. By influencing the absorption spectra of molecules, charged density, excitation energy, and photovoltaic characteristics, certain electronic excitations are impacted by the band gap. Chromophores with less frequent charge transfer typically exhibit larger band gaps.[37] Through excitations, higher LUMO and HOMO concentrations on the acceptor and donor parts facilitate the transfer of charge toward end-capped acceptors.

The electronegativity of atoms within molecules has a significant impact on electron delocalization as well. Changes in the energy levels of LUMO and HOMO can result from variations in the electronegativity of individual molecules. The OSCs' ability to transport charges efficiently can be affected by these energy-level adjustments. There may be a greater delocalization of electrons if there are more electronegative atoms with lower energy orbitals.[38] Figure 4 displays the charge density distribution of FMO, and Table 2 lists the HOMO−LUMO energy values together with the corresponding band gap values. The pink lobe represents areas with positive potential. On the other hand, the negative potential zones are represented by the green color lobe. Because of the smaller band gap in HNM2 and HNM5 molecules, the LUMO density is mostly found on the A2 acceptors of these compounds. From the donor region to the acceptor A2 region, these molecules transmit charge efficiently. Their LUMO and HOMO energy levels directly affect the efficiency, working capacity, and performance of the OSCs.

Table 2. Calculated HOMO−LUMO and E_g of the Synthetic Reference HNM and Designed HNM1−HNM8 Molecules

molecules	(E_{HOMO}) (eV)	(E_{LUMO}) (eV)	$E_g = E_{LUMO} - E_{HOMO}$ (eV)
HNM	−6.36	−2.67	3.69
HNM1	−6.83	−3.39	3.44
HNM2	−6.89	−3.47	3.41
HNM3	−6.54	−3.02	3.52
HNM4	−6.80	−3.37	3.43
HNM5	−6.69	−3.28	3.41
HNM6	−6.49	−2.95	3.54
HNM7	−6.79	−3.34	3.45
HNM8	−6.76	−3.30	3.46

With a band gap of 3.69 eV, the HNM molecule exhibits a HOMO at −6.36 eV and a LUMO at −2.67 eV, according to the listed statistics. In comparison to HNM, HOMO energy values for HNM1, HNM2, HNM3, HNM4, HNM5, HNM6, HNM7, and HNM8 are −6.83, −6.89, −6.54, −6.80, −6.69, −6.49, −6.79, and −6.76 eV. Every designed molecule has a higher LUMO value than HNM. From HNM1 to HNM8, these are arranged as −3.39, −3.47, −3.02, −3.37, −3.28, −2.95, −3.34, and −3.30 eV, respectively. It indicates that recently developed compounds are effective acceptor materials that could be combined with donor materials. HNM has a higher band gap value than all recently observed compounds. With values of 3.41, 3.41, 3.43, 3.44, 3.45, 3.46, 3.52, 3.54, and

https://doi.org/10.1021/acsomega.4c07436
ACS Omega 2024, 9, 44668−44688

3.69 eV, respectively, the rising band gap order of the examined molecules is HNM2 = HNM5 < HNM4 < HNM1 < HNM7 < HNM8 < HNM3 < HNM6 < HNM. Due to the presence of a nitro group at the terminal acceptor (A2), the HNM2 molecule exhibits the largest decrease in the band gap. Due to the presence of NO_2, CN, and COOH groups at the terminal acceptor (A2), the HNM5 also exhibits a low band gap. Because of these properties, electrons were effectively drawn toward the terminal atoms of these compounds.

When comparing the structures of HNM2 and HNM5, it can be seen that while their acceptors are slightly different, they are similar in that the HNM5′s acceptor has two COOH groups on its end side along with NO_2 and CN, whereas HNM2's acceptor has four NO_2 groups. HNM5′s acceptor has two more groups that can draw electrons than HNM2's do on terminal acceptors, which results in a greater energy reduction and becomes equal to HNM2. Although the structures of HNM3′s and HNM6's acceptors are similar, HNM3′s two electron-withdrawing fluorine atoms along with two NO_2 atoms on the terminal acceptors result in a greater band gap reduction than that observed with HNM6, which has two F atoms and two CN atoms. Better charge separation and improved photovoltaic absorption capabilities of these acceptors are also a result of these groups' notable electron-withdrawing abilities. In light of the band theory of energy, other closely examined molecules likewise show a decrease in band gap values as compared to HNM, leading to a convenient charge transition. This indicates that these chromophores are potentially useful for use as effective OSCs.

3.3. DOS Analysis. The extent to which various molecular components participate in HOMO and LUMO development is explained by the DOS assessment. The purpose of this study is to confirm the FMO evaluation's findings. It goes into detail on how much of Mullikan's charge disperses over the entire molecule.[39] Similarly, the DOS calculation determines the occupied and unoccupied molecular orbital energies of every fragment of the HNM1−HNM8 molecules. For a comprehensive analysis, each molecule is separated into three distinct groups based on its function: the end-group acceptors (A2), the donor subunit (D), and the core acceptor portion (A1). This section describes, in percentage form, how each component contributes to the energy levels of the HOMO and LUMO. The M062X functional at basis set 6-31G(d,p) of DFT was used to evaluate the DOS. PyMolyze 1.1 software was used to analyze Mullikan's charge density distribution, and Table 3 displays the final results.

There is a relative intensity displayed on the left side of the plots in the DOS graphs (Figure 5). In DOS plots, the orbitals' energies are displayed along the *x*-axis. The bottom *x*-axis is separated into three regions: the LUMO area is on the right side of the portion; the HOMO region is on the left side of the portion; and the band gap between the HOMO and LUMO energy levels is represented by the central planar part.

Additionally, different colored lines indicate how much each moiety in the molecules is involved. By way of comparison, the pink line represents the role of the terminal acceptors (A2), the green line represents the donor region (D), the orange line represents the core acceptor (A1), and the blue line represents the total contribution of all of the regions. The potential for each acceptor moiety to pull electrons toward itself is indicated by the distinct peaks of each molecule.

The donor portion of the HNM molecule contributes 33.3% to rising LUMO energy levels while having 64.9% participation

Table 3. Percentage of Acceptor A2, Donor D, and Core Acceptor A1 That Participated in the Distribution of HOMO and LUMO of Synthetic Reference HNM and Designed HNM1−HNM8 Molecules

molecules	FMO	acceptor (A2) (%)	donor (D) (%)	acceptor (A1) (%)
HNM	HOMO	15.8	64.9	19.3
	LUMO	18.2	33.3	48.5
HNM1	HOMO	17.6	62.5	19.9
	LUMO	49.4	31.5	19.0
HNM2	HOMO	16.8	62.7	20.5
	LUMO	55.1	29.1	15.9
HNM3	HOMO	15.6	64.6	19.8
	LUMO	44.0	31.3	24.7
HNM4	HOMO	16.7	62.9	20.4
	LUMO	52.4	30.1	17.5
HNM5	HOMO	17.3	63.2	19.5
	LUMO	52.9	30.3	16.8
HNM6	HOMO	16.4	64.3	19.3
	LUMO	37.1	33.4	29.5
HNM7	HOMO	17.6	62.6	19.8
	LUMO	47.9	32.1	20.1
HNM8	HOMO	17.5	62.8	19.7
	LUMO	47.0	32.0	21.0

in rising HOMO, according to Table 3 data. Nonetheless, the HOMO contribution of A1 and A2 acceptors is 19.3% and 15.8%, whereas the LUMO energy level is raised by central and terminal acceptors up to 48.5% and 18.2%. These details clarify that while the acceptor portions of the molecules mostly function at LUMO energy levels, the donor section of the molecule is noticeably involved in operating as HOMO. More charge mobility in the molecule will result from the roles of HOMO as a donor and LUMO as an acceptor, which will facilitate effective charge transport from donor to acceptor regions. The development of the HOMO and LUMO energy levels of the molecules is mostly facilitated by the donor and acceptor of each of the molecules under examination. Raising the HOMO energy level involves more of the donor region. The acceptor zone contributes more to the LUMO energy level, in comparison.

The donor contributions to HOMO are substantially higher for HNM3 and HNM6. These molecules have a higher density of HOMO charges in their donor region, as evidenced by the greater ability of their terminal acceptors to function as LUMO. Terminal acceptors, A2, are the main source of LUMO in molecules other than HNM3 and HNM6. Strong electron-withdrawing terminal acceptors in HNM3 and HNM6 have a higher capacity to draw electrons from the core areas. Therefore, the donor proportion is less likely to behave as a LUMO because of the presence of these strong electron-withdrawing moieties. One explanation for this could be the direct bonding of terminal acceptors to the donor section, which enables these molecules' uniform charge transfer from donor to acceptor regions.

The acceptors must play a significant role in the development of the molecules' LUMO to provide optimal charge transmission. Every designed molecule (HNM1−HNM8) contributes significantly to the development of LUMO energy levels; these molecules have effective charge transfer capabilities because of the electron-withdrawing moieties at the periphery. One may argue that the HNM2 molecule significantly influences how the LUMO area develops. The strong electron-withdrawing ability of HNM2 (55.1%) as opposed to that of HNM (18.2%) accounts for the percentage

https://doi.org/10.1021/acsomega.4c07436
ACS Omega 2024, 9, 44668−44688

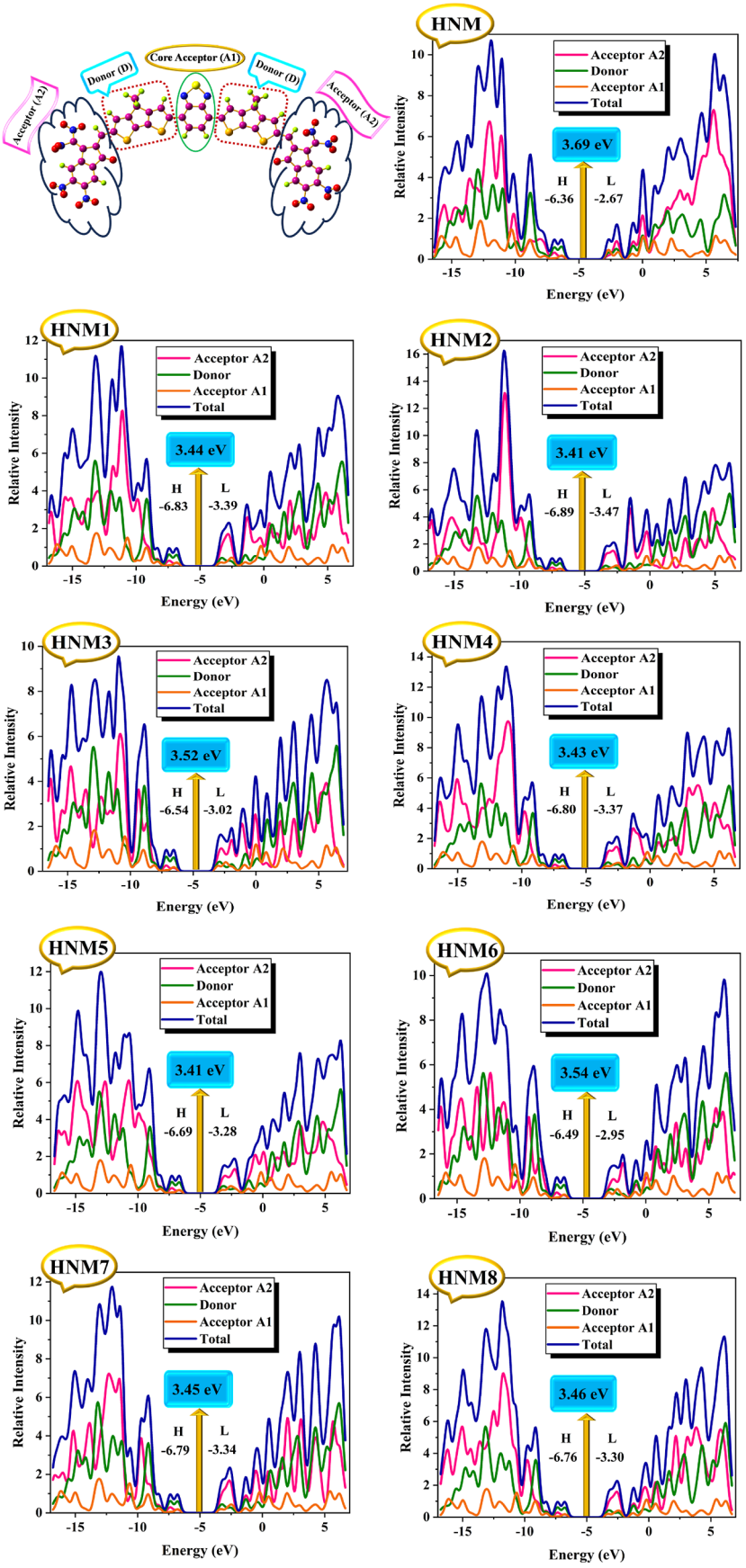

Figure 5. HOMO and LUMO densities and the energy difference of the synthetic reference HNM and designed HNM1−HNM8 molecules by DOS analysis.

https://doi.org/10.1021/acsomega.4c07436
ACS Omega 2024, 9, 44668−44688

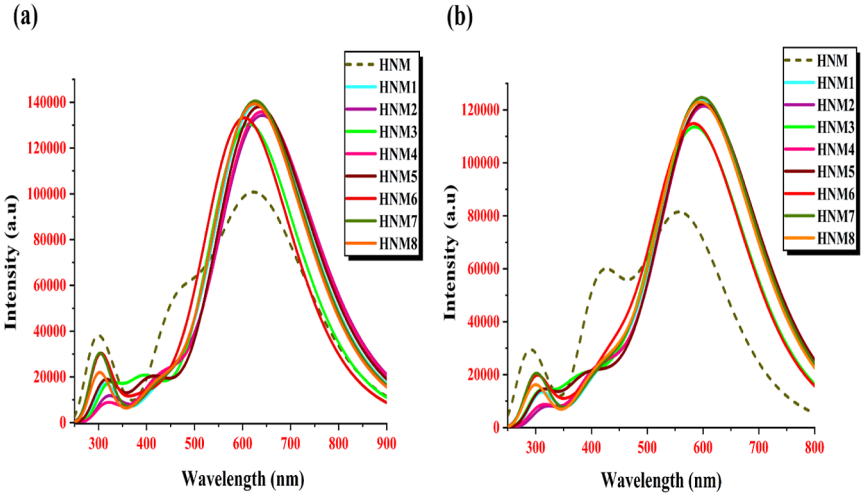

Figure 6. Comparison of UV−visible absorption (a) in the solvent (dichloromethane) phase for the synthetic reference HNM and designed HNM1−HNM8 molecules and (b) in the gas phase.

Table 4. Calculated UV−Visible Absorption, Excitation Energy (E_x), Oscillator Strength (f_{os}), and Major Molecular Orbital Assignments of the Synthetic Reference HNM and Designed HNM1−HNM8 Molecules in Dichloromethane Solvent

molecules	DFT calculated λ_{max} (nm)	experimental λ_{max} (nm)	E_x (eV)	f_{os}	major MO assignment
HNM	631.80	660	1.96	2.39	HOMO → LUMO (89%)
HNM1	635.72		1.95	3.26	HOMO →LUMO (72%)
HNM2	647.74		1.91	3.13	HOMO →LUMO (74%)
HNM3	619.92		2.00	3.04	HOMO →LUMO (76%)
HNM4	645.95		1.92	3.17	HOMO →LUMO(72%)
HNM5	641.31		1.93	3.21	HOMO →LUMO (73%)
HNM6	610.31		2.03	3.13	HOMO →LUMO (81%)
HNM7	633.83		1.96	3.28	HOMO →LUMO (75%)
HNM8	631.64		1.96	3.26	HOMO →LUMO (75%)

rise in the LUMO value of the acceptance terminal (A2). The observed increase in the percentage value of LUMO for the HNM1−HNM8 molecules indicates that the A2 acceptors of these developed compounds are more capable of withdrawing than HNM. Consequently, these compounds are a promising option for the synthesis of sophisticated OSCs.

3.4. Optical Property Analysis. Using the preestablished functional and basis states of TD-DFT, the absorptive characteristics of the molecules in both gaseous and solution states were determined. With the use of Origin 8.0, the absorption spectra of the molecules in both study phases were obtained, enabling us to discriminate between the values of maximum absorption of the various compounds under investigation, as indicated in Figure 6a,b. Along the *x*-axis, the wavelength was normalized along the intensity. Furthermore, Figure 6a,b displays line graphs that illustrate the difference between the two sets of results of λ_{max} in the solvent and gas phases, respectively. Tables 4 and 5 display the maximum absorption, oscillator strengths, excitation energies, and major MO assignment.

According to Figure 6b, the peak absorption of HNM and the tailored compounds HNM1−HNM8 were 562.49, 602.77, 606.25, 590.04, 606.02, 606.13, 587.52, 602.60, and 600.09 nm in the gas phase and 631.80, 635.72, 647.74, 619.92, 645.95, 641.31, 610.31, 633.83, and 631.64 nm, respectively, in the presence of the dichloromethane solvent (as shown in Figure 6a). Upon stabilization of the polar excited state by the polar solvent, all of the tailored compounds exhibited a significant solvent (near the IR) and a visible reddish-brown absorption

Table 5. Estimated UV−Visible Absorption, Excitation Energy, Oscillator Strength, and Major Molecular Orbital Assignments of the Synthetic Reference HNM and Designed HNM1−HNM8 Molecules in the Gas Phase

molecules	DFT calculated λ_{max} (nm)	E_x (eV)	f_{os}	major MO assignment
HNM	562.49	2.20	1.96	HOMO →LUMO (89%)
HNM1	602.77	2.06	2.97	HOMO →LUMO (79%)
HNM2	606.25	2.05	2.90	HOMO →LUMO (77%)
HNM3	590.04	2.10	2.72	HOMO →LUMO (81%)
HNM4	606.02	2.04	2.91	HOMO →LUMO (78%)
HNM5	606.13	2.05	2.92	HOMO →LUMO (73%)
HNM6	587.52	2.11	2.76	HOMO →LUMO (84%)
HNM7	602.60	2.06	2.98	HOMO →LUMO (80%)
HNM8	600.09	2.07	2.95	HOMO →LUMO (80%)

phase. The maximum wavelength in Figure 6a,b is provided by the solvent, which is because of higher conjugation in the solvent phase, even if the predicted absorption value of the designed molecules has shifted to a greater extent in both the gas phase and solvent. This higher conjugation could be the consequence of the chemicals' greater solvent solubility. The

https://doi.org/10.1021/acsomega.4c07436
ACS Omega 2024, 9, 44668−44688

maximum λ_{max} (606.25 and 647.74 nm in both investigated phases) of HNM2 is attributed to its tightly conjugated and electron-accepting component (presence of a nitro group at the end-capped). The order of absorption is HNM2 > HNM4 > HNM5 > HNM1 > HNM7 > HNM8 > HNM3 > HNM6 > HNM in the gaseous state, whereas in the solvent (dichloromethane) phase, it is HNM2 > HNM4 > HNM5 > HNM1 > HNM7 > HNM8 > HNM > HNM3 > HNM6.

The HNM3 and HNM6 molecules exhibit peaks to the left (blue shift). Both designed molecules show a blue shift, indicating that the molecule has a higher energy gap and absorbs light at shorter wavelengths. This inconsistency in shifting is due to the presence of two fluorine atoms at end-capped acceptor A2. This shows that structural modification has a major impact on energy levels and electronic transitions.

An important factor in determining whether a substance can be used in an organic photovoltaic cell is its excitation energy (E_x). As an electron jumps from its ground state (S_0) to its excited state (S_1), the energy used is indicated by E_x.[40] It is easier to excite an electron and to allow a charge to flow smoothly when the excitation energy is modest. A decrease in the E_x-values of HNM1−HNM8 in both solvent and gas phases, as compared to that of the HNM as shown in Tables 4 and 5, indicates the ability of the suggested molecules to efficiently transport electrons.

The molecule has a greater capacity for charge transfer, as evidenced by the smallest value for HNM2 of first excitation energy, narrower band gap (3.41 eV), and greater absorption maximum of 606.25 nm in the gas phase and 647.74 nm in solvent. The reason for this is that there is an electron-withdrawing acceptor entity that is potentiated. HNM2 has the potential to remain an active layer in efficient OSCs because of its low E_x (2.05 eV in the gas phase and 1.91 eV in the solvent phase). HNM3 and HNM6 have low wavelengths and high excitation energy as compared to the reference HNM in the solvent phase due to the presence of the fluorene group at the end-capped acceptor. There is no electron delocalization in fluorene and poor impact on the band gap, showing poor electronic and optical response as compared to other functional groups at the end-capped acceptor.

The frequency at which electrons in photovoltaic cells migrate from the ground HOMO levels to the stimulated LUMO levels is known as f_{os}. A stronger oscillator is produced by a higher f_{os}, which in turn indicates a higher charge transfer rate in the UV−visible zone. Tables 4 and 5 show that HNM and the designed chromophores HNM1−HNM8 have oscillator strengths in the ranges 2.98−1.96 in the gas phase and 3.28−2.39 in the solvent. The largest f_{os} and thus improved absorption and charge transformations are found in the HNM7 and HNM1 structures, with their strongest electron-deficient acceptor units at the terminal position.

3.5. Light-Harvesting Efficiency Evaluation. The ability of any photovoltaic molecule to receive and convert sunlight into electricity is measured by its LHE. The generation of J_{sc} is ultimately influenced by the strength of oscillators, which is strongly correlated with LHE. As a result, the capacity of solar devices to harvest sunlight has a significant impact on their efficiency.[41] The J_{sc} value is employed in the manufacturing of solar cell devices and is determined by utilizing eq 3.

$$J_{SC} = \int_{\lambda}^{0} \mathrm{LHE}(\lambda).\ \phi_{inj}\cdot\eta_{collect}\cdot \mathrm{d}\lambda \quad (3)$$

In this case, the electronic injection efficiency is denoted by ϕ_{inj}, while the total charge collection is represented by $\eta_{collect}$. Solar cells' photovoltaic efficacy is largely dependent on the J_{sc}. When there is no external resistance, it measures the highest current density that a solar cell can produce. J_{sc} is the maximum current that can be extracted from the solar cell depending on several variables. Equation 4 was utilized to compute the LHE of compounds that are now under study.[42]

$$\mathrm{LHE} = 1 - 10^{-f} \quad (4)$$

In the solvent phase of molecules, "f" represents the oscillator strength. Table 6 lists the calculated values for the LHE of the compounds under study.

Table 6. Calculated LHE of the Synthetic Reference HNM and Designed HNM1−HNM8 Molecules in Both the Solvent and the Gaseous Phases

molecules	f_{os} (solvent)	LHE (solvent)	f_{os} (gas)	LHE (gas)
HNM	2.39	0.9959	1.96	0.9890
HNM1	3.26	0.9995	2.97	0.9989
HNM2	3.13	0.9993	2.90	0.9987
HNM3	3.04	0.9991	2.72	0.9981
HNM4	3.17	0.9993	2.91	0.9988
HNM5	3.21	0.9994	2.92	0.9988
HNM6	3.13	0.9993	2.76	0.9983
HNM7	3.28	0.9995	2.98	0.9990
HNM8	3.26	0.9995	2.95	0.9989

These values are in the following ascending order: HNM < HNM3 < HNM2 = HNM4 = HNM6 < HNM5 < HNM1 = HNM7 = HNM8. In comparison to HNM, all investigated compounds exhibit better LHE. Modified molecules HNM1, HNM7, and HNM8 (0.9995 eV) show the highest LHE in the determined data because they have stronger oscillation strength than other molecules, as shown in Figure 7. One of the prerequisites for building effective devices in the future is satisfied by the enhanced LHE values of all newly introduced compounds.

3.6. Reorganization Energy Analysis. Photovoltaic cells' efficiency is based on how much energy is required to rearrange the electrons and holes in a molecule. Large charge mobilities are often permitted at low electron and hole reorganization energies and vice versa. Similar to electrons and holes, the mobility of a charge is inversely proportional to the energy needed to rearrange it.

Energy for rearrangement can be divided into two categories: internal energy (λ_{int}) and external energy (λ_{ext}). An internal reorganization may involve looking into all of the data related to a sudden change in the internal geometric symmetry. On the other hand, atmospheric variations can be interpreted as being expressed by external reorganizational power.[43]

Since the external environment does not cause any notable alterations, we will focus on only the energy consumed for λ_{int} in this case. This analysis is done using M062X with the 6-31G(d,p) basis set to examine the subtle reorganization energies of both the proposed HNM1−HNM8 and HNM molecules. The appropriate data are displayed in Table 7 and their comparisons are given in Figure 7.

For the HNM, the λ_e value is 0.0076. As shown in Table 7, the λ_e values for HNM1, HNM2, HNM3, HNM4, HNM5, HNM6, HNM7, and HNM8 are 0.0077, 0.0099, 0.0096,

https://doi.org/10.1021/acsomega.4c07436
ACS Omega 2024, 9, 44668−44688

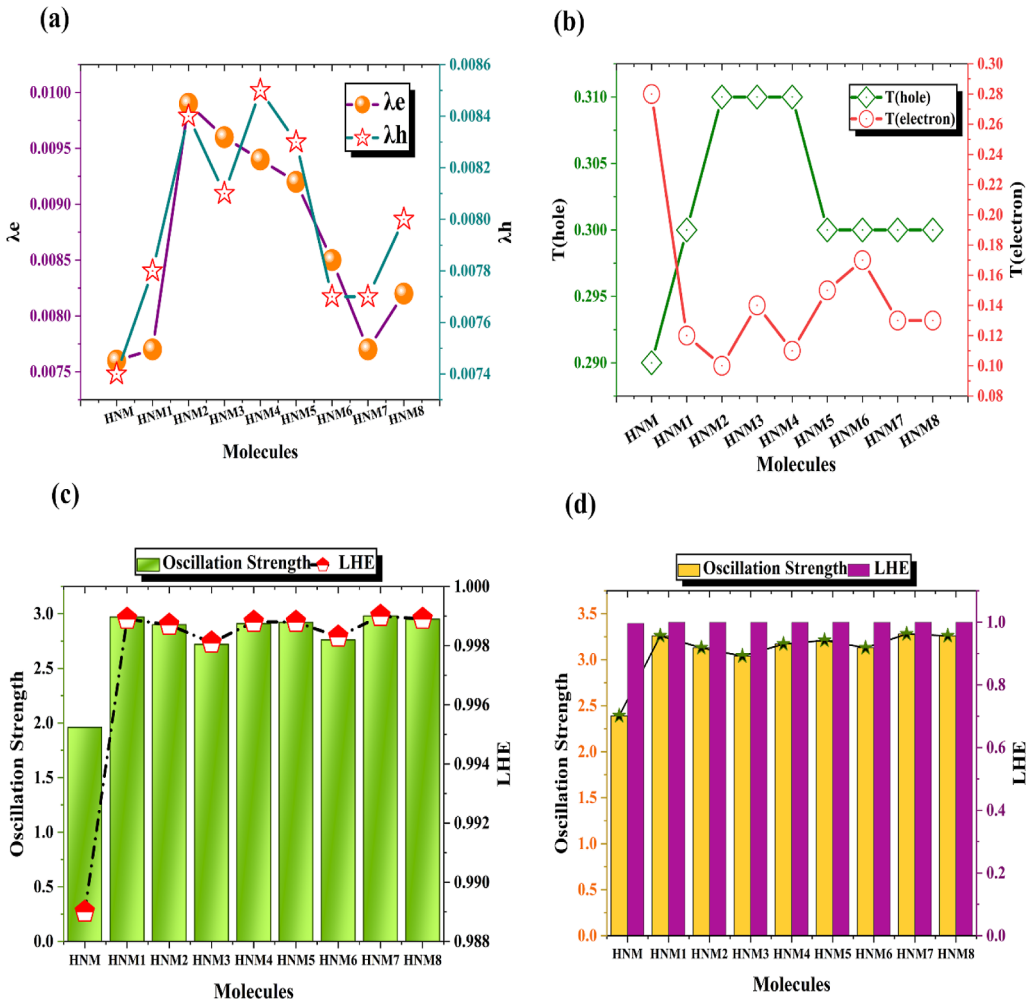

Figure 7. Comparative analysis of (a) reorganizational energies and (b) $T_{(hole)}$ and $T_{(electron)}$. (c) LHE and oscillator strength in the solvent phase (dichloromethane) and (d) in the gas phase of the synthetic reference HNM and designed HNM1−HNM8 molecules.

Table 7. Calculated λ_e, λ_h, T(hole), and T(electron) Values of the Synthetic Reference HNM and Designed HNM1−HNM8 Molecules

molecules	λ_e	λ_h	$T_{(hole)}$	$T_{(electron)}$
HNM	0.0076	0.0074	0.29	0.28
HNM1	0.0077	0.0078	0.30	0.12
HNM2	0.0099	0.0084	0.31	0.10
HNM3	0.0096	0.0081	0.31	0.14
HNM4	0.0094	0.0085	0.31	0.11
HNM5	0.0092	0.0083	0.30	0.15
HNM6	0.0085	0.0077	0.30	0.17
HNM7	0.0077	0.0077	0.30	0.13
HNM8	0.0082	0.0080	0.30	0.13

0.0094, 0.0092, 0.0085, 0.0077, and 0.0082, respectively, according to theoretical investigation. The value of λ_h for HNM is 0.0074. Theoretically, for HNM1, HNM2, HNM3, HNM4, HNM5, HNM6, HNM7, and HNM8, the values of λ_h are 0.0078, 0.0084, 0.0081, 0.0085, 0.0083, 0.0077, 0.0077, and 0.0080, respectively, as shown in Table 7. HNM6 and HNM7 molecules have the same λ_h value (0.0077). Consequently, their hole transport capacities are similar. In descending order, λ_h is as follows: HNM > HNM6 = HNM7 > HNM1 > HNM8 > HNM3 > HNM5 > HNM2 > HNM4. HNM4, HNM2, HNM5, and HNM3 are the best options for hole transfer, based on the sequence. RE's findings showed that our recently created BSe-based SCs were excellent candidates for highly efficient PSCs. These higher values from HNM are the outcome of our effective end-capped molecular engineering, which integrated effective functional groups (NO_2, SO_3H, COOH, and CN) and improved the materials' photovoltaic properties.

$T_{(hole)}$, often referred to as hole transport, is the ability of positively charged carriers or holes to move through the semiconductor material in a solar cell. Effective hole transport is necessary for the collection of holes at the electrode, which impacts the solar cell's overall performance. $T_{(electron)}$, sometimes termed electron transport, is the ability of negatively charged carriers, or electrons, to move through the semiconductor material of a solar cell. Efficient electron transport is necessary for the collection of electrons at the electrode, which is critical to the solar cell's successful operation. $T_{(hole)}$ values of HNM and HNM1 are 0.29 and 0.30, respectively. HNM2, HNM3, and HNM4 have the same $T_{(hole)}$ values (0.31), while HNM5, HNM6, HNM7, and HNM8 have the same values of $T_{(hole)}$ (0.30). $T_{(electron)}$ value of HNM is 0.28. From HNM1 to HNM8, the $T_{(electron)}$ values are 0.12, 0.10, 0.14, 0.11, 0.15, 0.17, 0.13, and 0.13. Both $T_{(hole)}$ and $T_{(electron)}$ values are shown in Table 7 and their relation is shown in Figure 7. $T_{(hole)}$ and $T_{(electron)}$ are important factors in solar cell research because

https://doi.org/10.1021/acsomega.4c07436
ACS Omega 2024, 9, 44668−44688

they directly affect the overall charge transport and collecting efficiency inside the device. Comprehending and refining these transport characteristics are essential to increasing the PCE of OSCs and reducing energy losses via recombination.

3.7. Open Circuit Voltages Investigation. When determining the photovoltaic characteristics of NFA-based organic photovoltaic devices, open circuit voltage (V_{oc}) plays a significant role. When the photovoltaic device operates at zero current, this is the highest voltage that can be extracted. Many variables, including device temperature, molecular energy levels, light intensity, and charge-carrier recombination, affect the open circuit voltage. The comparison of the HOMO and LUMO values yields the maximum value for V_{oc}. To get the value of V_{oc}, the acceptor's LUMO must be higher and the donor's HOMO energy value must be smaller. This reduces the band gap, which is an ideal situation for solar cells from all angles. In this case, a lower HOMO value correlates with negative values, which increase the actual HOMO value as they get smaller and vice versa. This also applies to LUMO. Reduced band gaps increase absorption, which raises the effectiveness of light harvesting and V_{oc}. However, while increased absorption can potentially enhance the short-circuit current, it often comes at the expense of lower V_{oc}. The efficiency of OSCs is directly correlated with their photovoltaic parameters (V_{oc}, FF, and J_{sc}); the greater the V_{oc} content, the better the efficiency.[44] Figure 8 provides a visual illustration of a comparison between the acceptor molecule's LUMO and the donor polymer PTB7-Th's HOMO to determine V_{oc}. The V_{OC} can be calculated quantitatively by applying the following eq 5.[45]

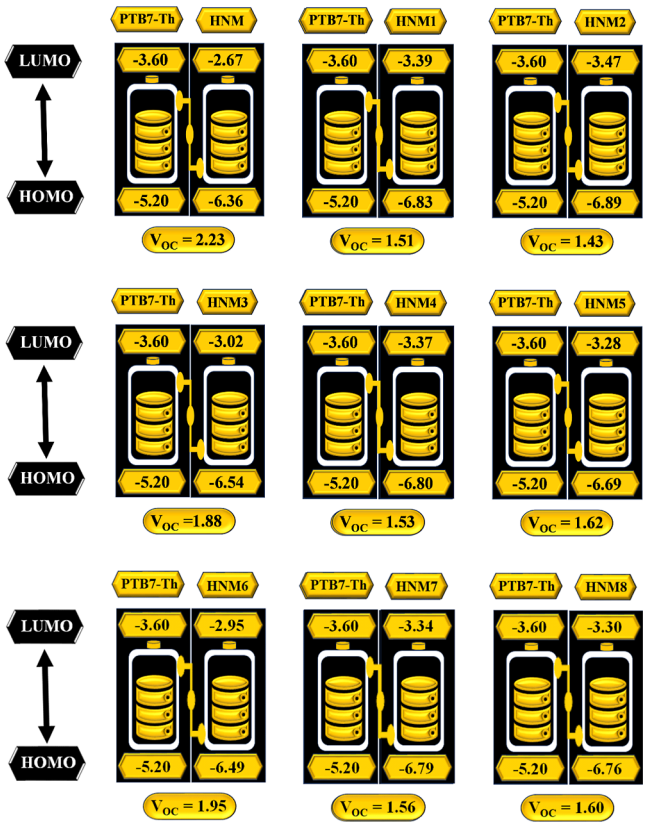

Figure 8. Calculated V_{OC} of the synthetic reference HNM and designed HNM1−HNM8 molecules with polymer donor PTB7-Th.

$$V_{OC} = (|E^{D}_{HOMO}| - |E^{A}_{LUMO}|) - 0.3 \quad (5)$$

Here, E stands for the energy of the used FMOs and 0.3 for empirical factors, which are likewise constant for every molecule. For HOMO and LUMO, PTB7-Th has values of −5.20 and −3.60 eV, respectively. Table 8 presents the computed open circuit voltage values for the reference molecule HNM and built compounds (HNM1−HNM8).

Table 8. Estimated V_{oc} and FF Values of the Synthetic Reference HNM and Designed HNM1−HNM8 Molecules

molecules	V_{oc}	FF
HNM	2.23	0.9487
HNM1	1.51	0.9349
HNM2	1.43	0.9328
HNM3	1.88	0.9428
HNM4	1.53	0.9352
HNM5	1.62	0.9375
HNM6	1.95	0.9442
HNM7	1.56	0.9360
HNM8	1.60	0.9370

These values are 2.23, 1.15, 1.43, 1.88, 1.53, 1.62, 1.95, 1.56, and 1.60 V. Because the LUMO level values for the proposed molecules (HNM1−HNM8) are higher than that of HNM, the computed value of V_{OC} for these compounds is smaller than that of HNM. The V_{OC} values for the proposed compounds are observed as follows, in decreasing order, according to $HOMO_{PTB7\text{-}Th}$−$LUMO_{acceptor}$ band gap: HNM > HNM6 > HNM3 > HNM5 > HNM8 > HNM7 > HNM4 > HNM1 > HNM2.

The appropriateness of complex interfaces, or E_{LL}, is another aspect that influences the efficiency. It is the distinction between the acceptor molecule's LUMO and the donor polymer's LUMO. According to published research, the optimal E_{LL} value for effectively injecting electrons from the donor to the acceptor is anywhere between 0.2 and 1 eV. As seen in Table 9, the E_{LL} values for the customized acceptor in this investigation range from 0.13 to 0.93 eV. E_{LL} values can be calculated by using eq 6 theoretically.

$$E_{LL} = L_D - L_A \quad (6)$$

Table 9. Computed Values of E_{LL} and E_{CT}, Energy Loss Incurred during Charge Generation, and Energy Loss Incurred during Charge Recombination for the Synthetic Reference HNM and Designed HNM1−HNM8 Molecules

molecules	E_{LL} (eV)	E_{CT} (eV)	energy loss incurred during charge generation	energy loss incurred during charge recombination
HNM	0.93	2.53	1.16	0.30
HNM1	0.21	1.81	1.63	0.30
HNM2	0.13	1.73	1.69	0.30
HNM3	0.58	2.18	1.34	0.30
HNM4	0.23	1.83	1.60	0.30
HNM5	0.32	1.92	1.49	0.30
HNM6	0.65	2.25	1.29	0.30
HNM7	0.26	1.86	1.59	0.30
HNM8	0.30	1.90	1.56	0.30

https://doi.org/10.1021/acsomega.4c07436
ACS Omega 2024, 9, 44668−44688

The E_{CT} value of HNM is 2.53, as shown in Table 9. The E_{CT} values of HNM and HNM1−HNM8 acceptors can be calculated theoretically by using eq 7.

$$E_{CT} = L_A - H_D \tag{7}$$

Computation is done on energy loss generation and combination using $E_{CT}-E_g$ and $E_{CT}-V_{OC}$, respectively. The interfacial charge transfer (E_{CT}) demonstrates the effectiveness of the donor−acceptor interface and the suitability of the donor polymer used.

3.8. Electrostatic Potential Analysis. We can comprehend the charge separation within a molecule using electrostatic potential (ESP) calculations. It excludes polarization and charge transfer to measure the unit charge at a specific point. The best representation of how molecules interact electrostatically with their external surroundings is determined by this parameter.[46] Studies of the distribution of energy in both organic and inorganic compounds as well as their reactivity are aided by ESP analysis. Through the manifestation of sites that are open to electrophilic and nucleophilic attacks, the ESP reveals the presence of more and fewer electronegative atoms through their respective negative and positive potentials. This information facilitates the comprehension of electronic densities and hydrogen bonds.[47] Electrophiles can initiate an attack when the electron-rich region is revealed by red saturation in the ESP maps. Nucleophilic attack is further made easier by the low electron density areas, which are indicated by the blue tone. This makes it remarkable that because oxygen, sulfur, and nitrogen atoms are electronegative, a negative potential is focused at these locations.

Compared with nitrogen and oxygen, the sulfur atom is less electronegative and has a lower negative potential. The positive potential of hydrogen atoms is also demonstrated by their blue enrichment,[48] as Figure 9. illustrates. The improved distinction between the red and blue hues shows how electrons are transferred from the donor to the terminal acceptors, keeping a specific distance. Higher-dipole-moment molecules exhibit this color separation more frequently, which contributes to the specific sites' strong reactivity. Using different shades, this study explores HNM and all newly proposed molecules (HNM1−HNM8) to elaborate on the electron-rich and -poor locations. The donor sites, which are richer in electrons and open to attack by electrophiles, are represented by the color blue. As each molecule's terminals are indicated in red to indicate the presence of acceptor moieties, Figure 9 illustrates that the donor sites of all the molecules under study have a higher electron concentration. The cyanide groups in some designed molecules are where the majority of the red color is concentrated. Similar to this, a positive potential is found at the donor site of all given molecules, while its more negative potential is found on the dicyanide groups and other electron-withdrawing groups of all compounds. As a result, these maps demonstrate that these molecules' excellent charge separation is advantageous to the performance of OSCs.

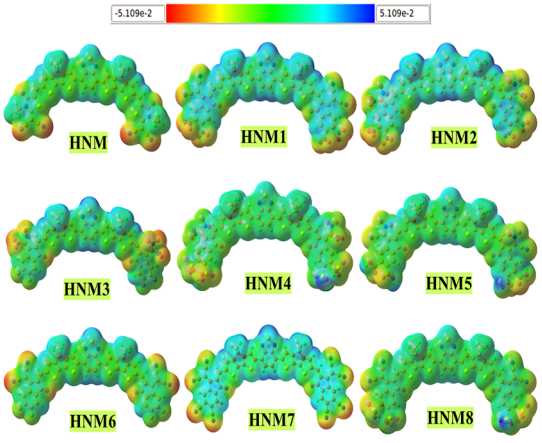

Figure 9. Electrostatic potential maps of the synthetic reference HNM and designed HNM1−HNM8 molecules.

3.9. Transition Density Matrix Analysis. Predicting the qualitative data on the movements of two-dimensional excitons (electron−hole pairs) inside the conjugate geometry of molecules is necessary for TDM analysis. Electromobility during the excitation phenomena, charge transitions, and charge locations can all be examined with this approach. A TDM plot is typically used to gain a complete understanding of the charge's mobility within the molecule as well as the degree of delocalization and resonance.

As hydrogen atoms have little effect on charge-transfer capabilities, their participation is disregarded. Atomic sequence (except from H atoms) is shown by the left *y*-axis and bottom *x*-axis of the molecule.[49] The charge density coefficient is displayed by the multicolored bar on the right *y*-axis. For the purpose of the transition pathway, the molecules were separated into three parts according to the function of each component found in the molecule. The constituent components were identified as core acceptors (A1), donor components (designated D), and terminal acceptors (A2). The electron density is distributed throughout the entire molecule in all of the reference HNM and closely examined molecules (HNM1−HNM8), as seen in Figure 10.

In these graphs, the strong dispersion along the diagonals displays hole and electron coherence in the donor and terminal acceptor units. The several transition points are shown by the diagonal bright patches. A smooth and effective transfer of electrons is achieved through the following conjugation, which causes charge to disperse from donor regions to acceptor regions.[50] This implies that all created compounds may have easier and more significant exciton dissociation in the excited state, even if they all have lower electron couplings than the reference molecule. All of the compounds we produced showed effective spectrum transitions compared to HNM, indicating their hidden potential as a photoactive material for future efficient device development.

3.10. Exciton Binding Energy Analysis. A crucial factor in the analysis and assessment of OSCs is their exciton binding energy (E_b). It signifies the force needed to separate the charge carriers once they have formed a connected pair (exciton). The Coulombic interaction intensity between the electron and the hole determines this, E_b. Charge carriers with lower E_b values can therefore easily move in the direction of any electrode. We may calculate the binding energy of the chemicals under study in theory by using eq 8.[51]

$$E_b = E_{H-L} - E_{opt} \tag{8}$$

Here, E_{H-L} is band gap E_g, and the excited molecules' excitation energy is designated as E_{opt}. In the gas phase, the values for E_b of HNM and all other formulated structures HNM1−HNM8 are 1.48 1.38, 1.37, 1.42, 1.38, 1.37, 1.43, 1.39, and 1.40 eV; in the solution phase (dichloromethane), the values are 1.73 1.49, 1.50, 1.52, 1.51, 1.48, 1.51, 1.49, and

https://doi.org/10.1021/acsomega.4c07436
ACS Omega 2024, 9, 44668−44688

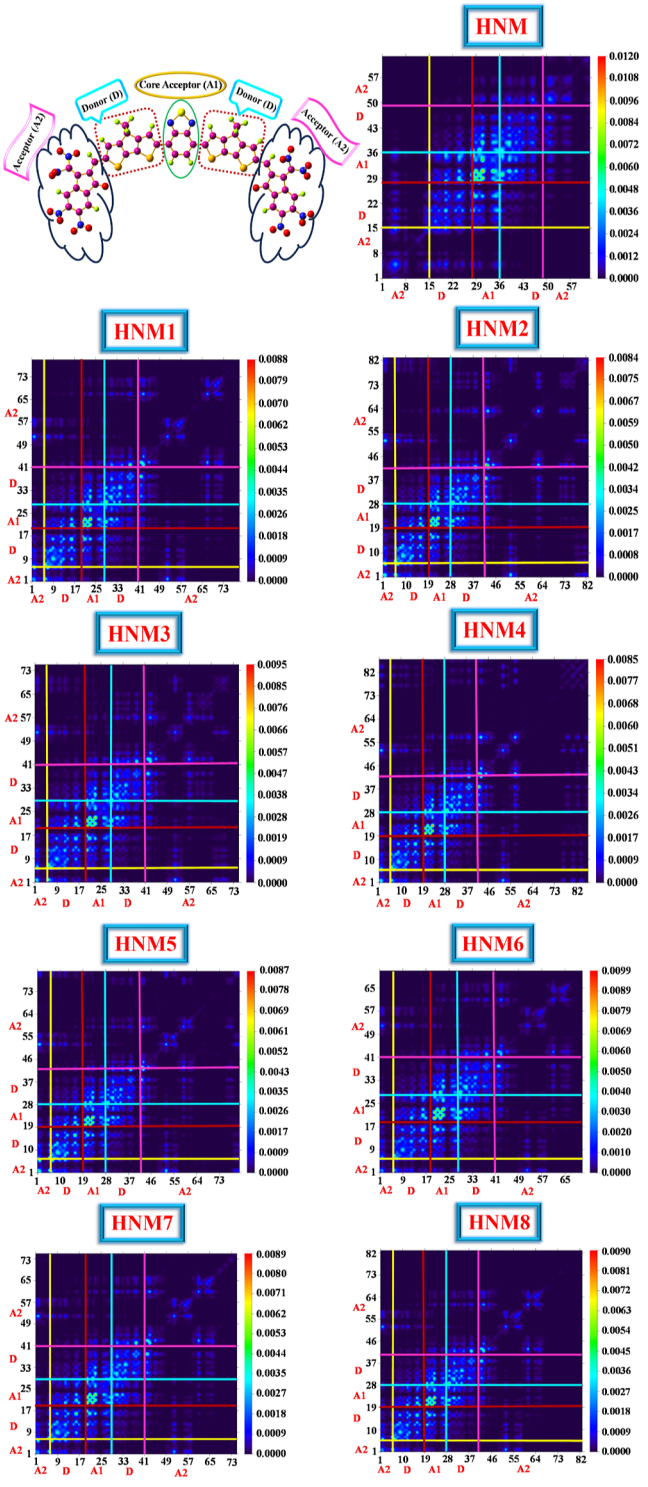

Figure 10. Transition density matrix maps of the synthetic reference HNM and designed HNM1−HNM8 molecules.

1.50 eV, respectively. HNM > HNM6 > HNM3 > HNM8 > HNM7 > HNM1 = HNM4 > HNM5 = HNM2 in the gas phase and HNM > HNM3 > HNM4 = HNM6 > HNM8 = HNM2 > HNM7 = HNM1 > HNM5 in dichloromethane are the sequences in which the binding energies of all the compounds are based, according to Figure 12. This sequence makes it evident that all designed molecules have low binding energy values compared to the reference HNM in both gas and solvent dichloromethane. This indicates that these compounds have a higher potential for exciton dissociation. Therefore, these molecules may have the capacity for significant charge mobility based on exciton E_b data.

3.11. Heat Maps Analysis. A set of molecules with the labels HNM1-HNM8 and HNM have had their electron and hole overlaps theoretically computed. Figure 11 displays the generated graphs. Plot analysis shows that there is significant electron−hole overlap in all designed compounds. There is a noticeable amount of electron and hole overlap in every molecule. The HNM2-labeled molecule shows very high-intensity overlap and a small energy gap, together with robust electron and hole mobility.

3.12. Ionization Potential and Electron Affinity Analysis. The breakdown of the oxidation and reduction potentials, respectively, yielded the IP and EA of these compounds. The degree of charge transfer within molecules is efficiently coordinated by these characteristics. Because the HOMO is destabilized, molecules with electron-donating groups maintain a lower IP, which facilitates the removal of electrons. Thus, by reducing the energy of the HOMO, EWGs cause stability in that particle. As a result, it is difficult and energy-intensive to remove an electron from a HOMO. On the other hand, its stability encourages donor electron absorption through the acceptor moiety. Eqs 9 and 10 ascertain the IP and EA.[52]

$$\mathrm{IP} = [E_0^+ - E_0] \tag{9}$$

$$\mathrm{EA} = [E_0 - E_0^-] \tag{10}$$

Table 10 provides an overview of all compounds' IP and EA values, and Figure 12 shows their relation. In this study, every molecule under investigation has the rising order of IP as HNM (6.65 eV) < HNM6 (6.76 eV) < HNM3 (6.81 eV) < HNM5 (6.94 eV) < HNM8 (7.01 eV) < HNM7 (7.04 eV) < HNM4 (7.05 eV) < HNM1 (7.08 eV) < HNM2 (7.14 eV). This order shows that all molecules have higher IP values than the HNM. Electron shifting toward LUMO has been made easier by the acceptor moiety connected to the terminals of molecules, which has greatly increased the energy of HOMO. According to this, molecules with EA values higher than that of the reference molecule exhibit faster electron-acceptance from donors by accelerating the electrophilic activity of the molecules. The trend of higher EA in all chemicals studied is as follows: HNM (2.33 eV) < HNM6 (2.64 eV) < HNM3 (2.71 eV) < HNM5 (2.97 eV) < HNM8 (3.00 eV) < HNM7 (3.05 eV) < HNM4 (3.08 eV) < HNM1 (3.09 eV) < HNM2 (3.16 eV). These statistics show that, compared to reference, all molecules are better electron acceptors. The development of better solar devices may emerge from the results, which show that molecules intended for charge transfer have better and improved capabilities.

3.13. Chemical Reactivity Exploration. The reactivities of acceptor and donor molecules can be inferred from the values of five primary factors. The direction of charge transfer from one molecule to another is likewise specified by these parameters. These are the following: electronegativity (χ), chemical potential (μ), chemical softness (S), chemical hardness (η), and electrophilicity index (ω). To gain an understanding of chemical reactivity, we computed these values using eqs 11−16.[53]

The propensity of an acceptor to pick up a negative charge is known as its chemical potential (μ). It is the molecule's ability to donate electrons for a donor. Table 10 contains the

https://doi.org/10.1021/acsomega.4c07436
ACS Omega 2024, 9, 44668−44688

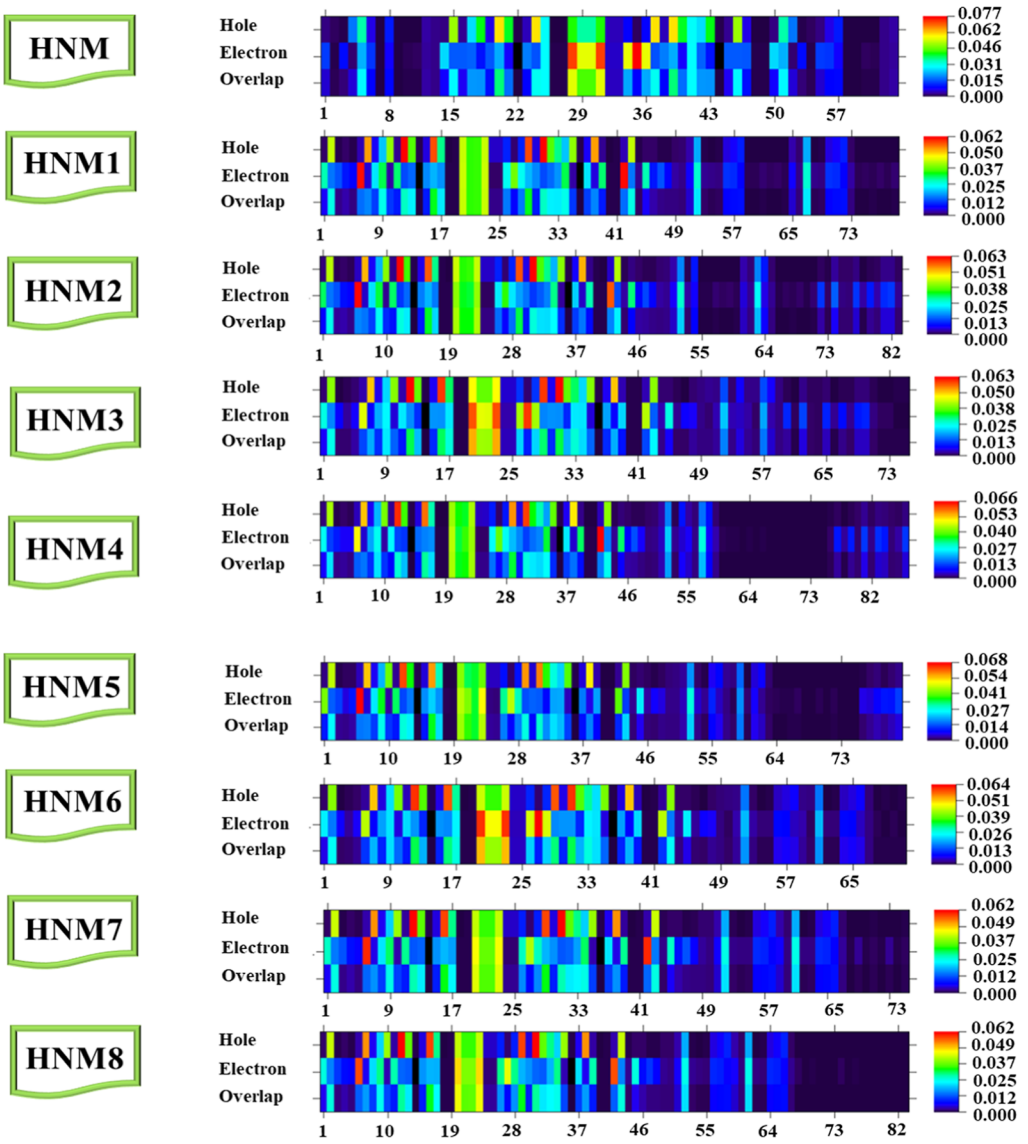

Figure 11. Hole−electron-overlap surfaces of the synthetic reference HNM and designed HNM1−HNM8 molecules.

computed chemical potentials for HNM1−HNM8 along with reference HNM using eq 11.

$$\text{Chemical potential } (\mu) = \frac{[E_{\text{LUMO}} + E_{\text{HOMO}}]}{2} \tag{11}$$

Chemical softness (S) and hardness (η), which are inversely related, also affect the chemical potential. These parameters, which we determined using eqs 12 and 13, are shown in Table 10

$$\text{chemical hardness } (\eta) = \frac{[E_{\text{LUMO}} - E_{\text{HOMO}}]}{2} \tag{12}$$

$$\text{chemical softness } (S) = \frac{1}{\eta} \tag{13}$$

Because there is less resistance, smooth electron transfer is caused by a higher softness. All of our recently produced compounds (HNM1−HNM8) exhibit stronger softness than the reference, as shown by the softness values in Table 10. Figure 12 shows a comparative analysis between softness and hardness. The softness of HNM1−HNM8 is significantly improved, with respective values of 0.58, 0.59, 0.57, 0.58, 0.59, 0.56, 0.58, and 1.00 eV, while the softness value of reference HNM is less than those of all designed compounds, i.e., 0.54 eV. This demonstrates the likelihood of an increased charge transfer rate in these engineered molecules, supporting the efficacy of our end-capped designing method. By reducing the hardness, the other newly created molecules likewise exhibit improved softness. This could be as a result of end-capped acceptor designing, which improved the interactions between different molecular components, which raises the charge transfer process.

Electrophilicity (ω) and electronegativity (χ) account for excessive electron flow. The direction of electron flow is ascertained by the values obtained from eqs 14 and 15

$$\text{electro negativity } (\chi) = -\frac{[E_{\text{LUMO}} + E_{\text{HOMO}}]}{2} \tag{14}$$

$$\text{electro philicity Index } (\omega) = \frac{\chi^2}{2(\eta)} \tag{15}$$

https://doi.org/10.1021/acsomega.4c07436
ACS Omega 2024, 9, 44668−44688

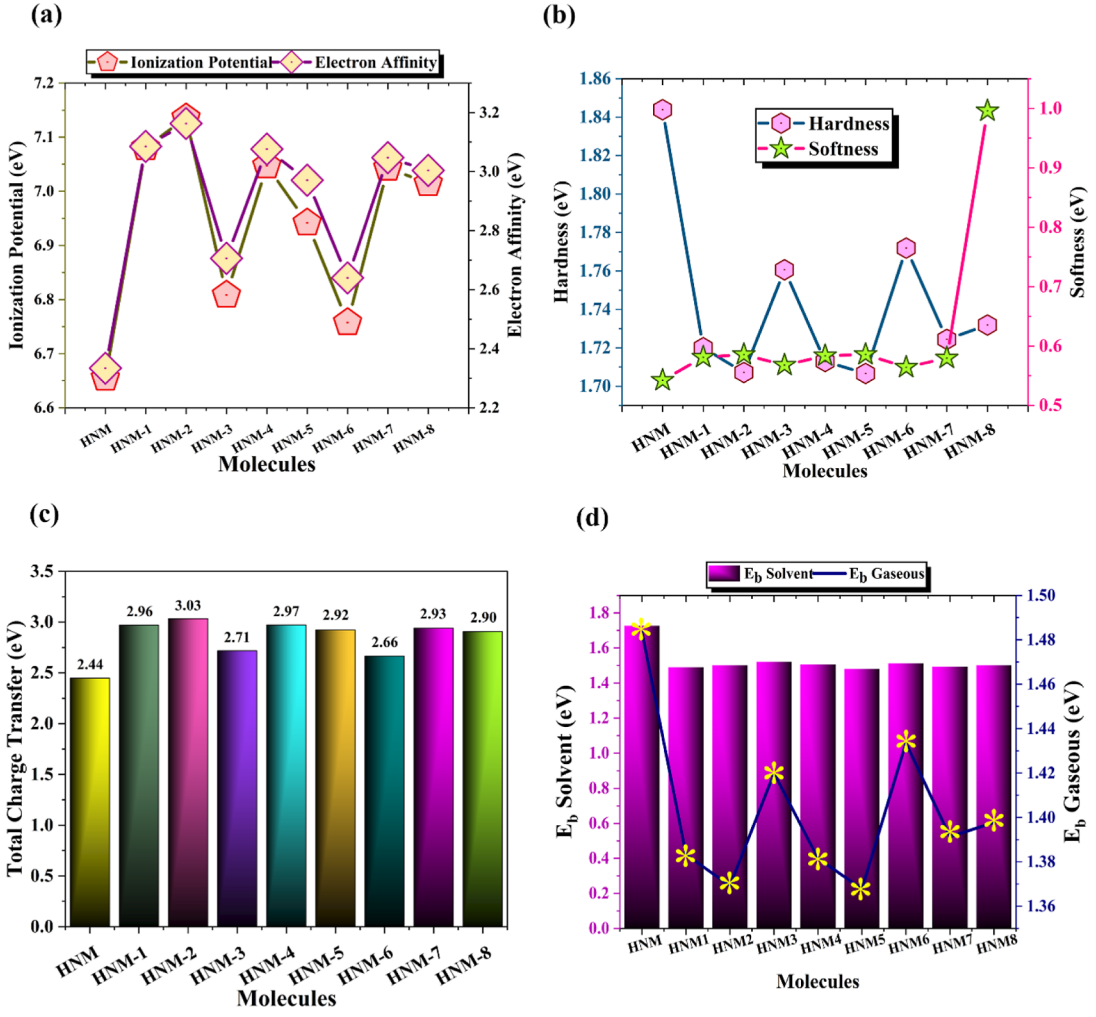

Figure 12. Comparative analysis of (a) IP and EA and (b) softness and hardness. (c) Illustration of the total amount of charge transfer and (d) comparative analysis of binding energy between solvent (dichloromethane) and gaseous phases of the synthetic reference HNM and designed HNM1−HNM8 molecules.

Table 10. IP, EA, and Chemical Reactivity Parameters of the BSe-Based HNM Reference and HNM1−HNM8 Acceptors

molecules	IP (eV)	EA (eV)	μ (eV)	η (eV)	S (eV)	χ (eV)	ω (eV)	ΔN_{max} (eV)
HNM	6.65	2.33	−4.51	1.84	0.54	4.51	5.53	2.45
HNM1	7.08	3.09	−5.11	1.72	0.58	5.11	7.59	2.97
HNM2	7.14	3.16	−5.18	1.71	0.59	5.18	7.85	3.03
HNM3	6.81	2.71	−4.78	1.76	0.57	4.78	6.49	2.72
HNM4	7.05	3.08	−5.09	1.71	0.58	5.09	7.56	2.97
HNM5	6.94	2.97	−4.99	1.71	0.59	4.99	7.28	2.92
HNM6	6.76	2.64	−4.72	1.77	0.56	4.72	6.28	2.66
HNM7	7.04	3.05	−5.07	1.72	0.58	5.07	7.45	2.94
HNM8	7.01	3.00	−5.03	1.73	1.00	5.03	7.31	2.91

$$\text{total amount of charge transfer } (\Delta N_{max}) = -\frac{\mu}{\eta} \quad (16)$$

Table 10 shows that, in comparison to the other compounds, HNM1, HNM2, and HNM4 have a larger tendency for electrons with higher ω values of 7.59, 7.85, and 7.56 eV. High electronegativity of HNM1 (5.11 eV), HNM2 (5.18 eV), and HNM4 (5.09 eV) indicates a greater capacity to take electrons from donor molecules. Equation 16 measures the total amount of charge transfer (ΔN_{max}), and its graphical illustration is given in Figure 12 for all developed HNM1−HNM8 acceptors along with the HNM reference. Along the *y*-axis, the total amount of charge transfer for each molecule is given. The highest value of all the developed compounds is 3.03 for HNM2. For the future development of effective OSCs, these characteristics of the molecules listed make them a better option.

3.14. Fill Factor Evaluation. Any photovoltaic device's efficiency in converting light to energy is directly impacted by its fill factor. The open circuit voltage is mostly responsible for it. The fill factor will rise in proportion to the higher value of V_{OC}, which will likewise raise the device's photovoltaic performance. The fill factor's optimum and ideal value is

https://doi.org/10.1021/acsomega.4c07436
ACS Omega 2024, 9, 44668−44688

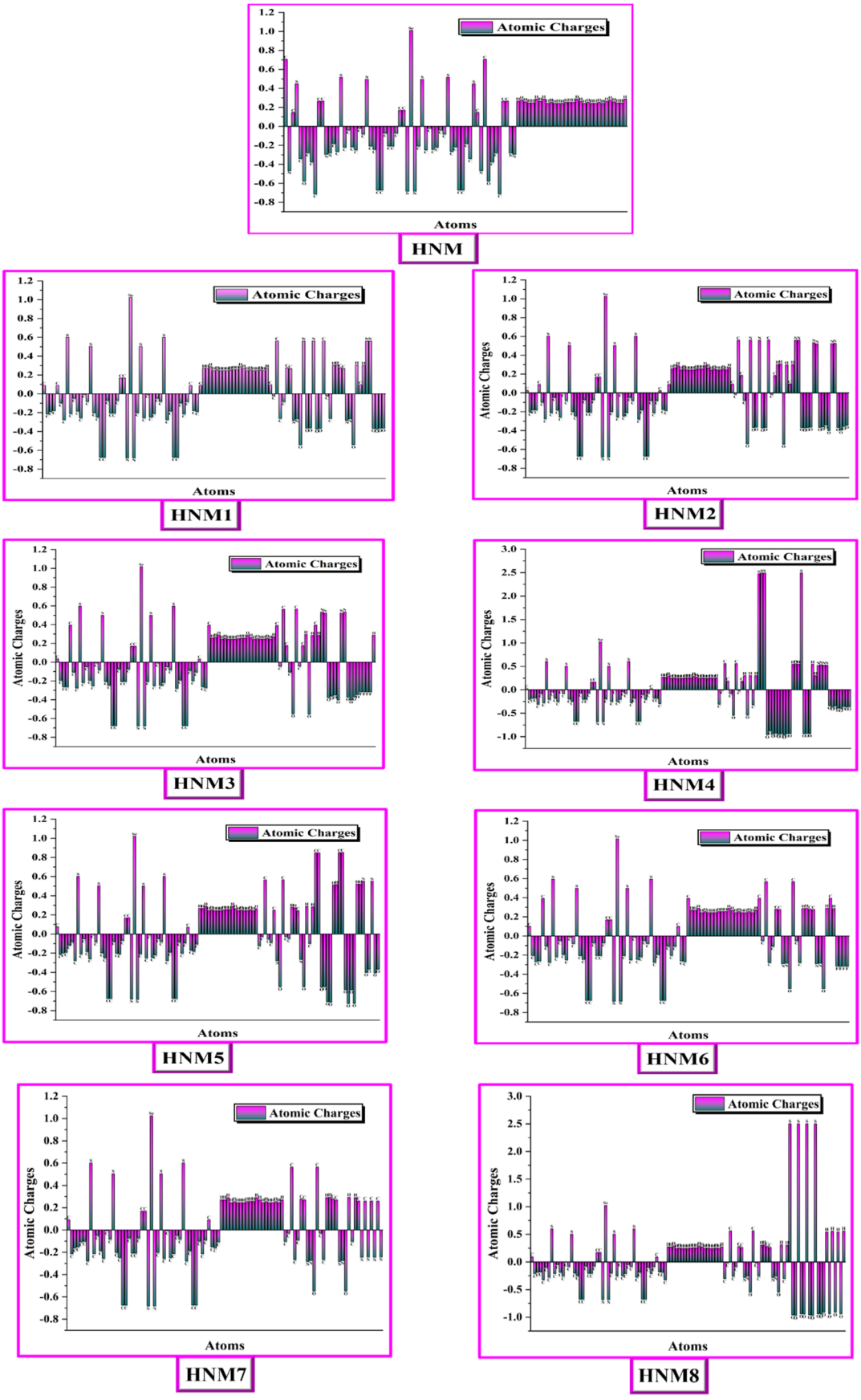

Figure 13. Natural population analysis of the synthetic reference HNM and designed HNM1−HNM8 molecules.

https://doi.org/10.1021/acsomega.4c07436
ACS Omega 2024, 9, 44668−44688

unity, or 100%. To get the fill factor of HNM and all optimal intended molecules, we utilized eq 17.[54]

$$FF = e\frac{V_{OC}}{K_B T} - \frac{\ln\left(e\frac{V_{OC}}{K_B T} + 0.72\right)}{\frac{eV_{OC}}{K_B T} + 1} \quad (17)$$

The temperature, T, is fixed at 300 K, the elementary charge, e, is represented in $e\frac{V_{OC}}{K_B T}$, which is fixed at 1, and the Boltzmann constant, K_B, is $8.61733034 \times 10^{-5}$ eV/K. As can be seen from Table 8, all of the suggested molecules have FF values that are nearly equal to the optimum value for FF: 0.9349 for HNM1, 0.9328 for HNM2, 0.9428 for HNM3, 0.9352 for HNM4, 0.9375 for HNM5, 0.9442 for HNM6, and 0.9360 and 0.9370 for HNM7 and HNM8, respectively. These molecules emerge as viable options as a result of this work; attention should be paid to them in order to create effective solar cells in the future.

3.15. Natural Population Analysis. The atomic charges and electron distribution of substances can be determined with great efficiency using NPA.[55] The net atomic charges of the A2-D-A1-D-A2 designed molecules are shown in Figure 13, as calculated by natural population analysis. Because hydrogen atoms are close to sulfur, nitrogen, and carbon atoms, hydrogen has a positive charge. Except for the carbon atoms attached to the electronegative nitrogen, fluorine, sulfur, selenium, and oxygen atoms, every carbon atom in the donor and acceptor is negatively charged.

Because they are bonded to positively charged carbon and hydrogen, all nitrogen atoms are negatively charged. As HNM1 and HNM2 show, nitrogen has a positive charge that is coupled to oxygen. Like hydrogen and carbon, all oxygen atoms have a negative charge and are detected. Sulfur is coupled to electronegative nitrogen and oxygen with a positive charge and is found in the acceptor zone as well as the donor part. Negatively charged nitrogen, oxygen, fluorine, and carbon are the causes of charge delocalization in the studied BSe-based acceptors HNM and HNM1 to HNM8, according to Mulliken charge analysis. The positive charge of the nitrogen, sulfur, hydrogen, and carbon atoms contributed to the asymmetric distribution as well. According to the description above, electrons are transferred from the donor to the acceptor moieties. Therefore, molecules are employed as an effective material for OSC devices, and acceptor modification is an effective method for achieving a charge separation state in the molecules under investigation.

3.16. Electron Density Difference Analysis. Understanding the division of the excited state exciton and charge separation can be achieved by the application of an EDD analysis between the ground states and the excited states. Figure 14 shows the charge densities for each of the structures under study. Different colors on EDD maps represent different electron densities in different locations. Based on EDD maps of the studied molecules, the region of holes (shown in green) zone of electron reduction is centered on the donor group. Conversely, the orange color indicates that the electron density is confined in the acceptor pieces of all the molecules under study. Plots of EDD maps indicate that intramolecular charge transfer (ICT) is similar in all series of compounds and that ICT transfers from the donor toward the terminal acceptor fragments in all compounds under consideration.[56] Consequently, it may be said that the compounds under investigation can serve as efficient acceptor materials for OSCs.

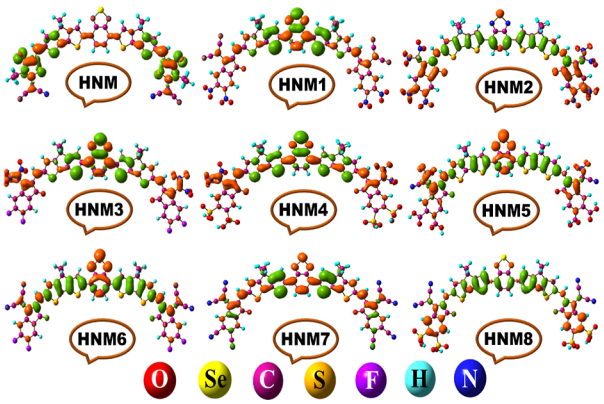

Figure 14. EDD surfaces analysis of the synthetic reference HNM and designed HNM1−HNM8 molecules.

EDD parameters are used to quantify the existence of holes and electrons, as shown in Table 11. Reduced electron density is observed during electron transition as the t-index value of all molecules is less than zero. So negative t-index shows more charge (hole) transfer. These negative t-index values indicate that all molecules act as good acceptors due to the accepting density during excitation of charges (electron and hole). The t-index values of HNM2 and HNM are −5.96 and −2.48, respectively. Our developed molecules show higher H index (hole-index) and lower D index (donor-index) values. This indicates the presence of more hole-density during excitation, and all molecules act as reservoirs of positive charge, so they are good acceptors. The hole part of molecules combines with the negative part of the donor for a smooth flow of charges during the charge transfer process. H index values of all molecules lie between 4.95 and 10.35. HNM2 has a higher H index value, i.e., 10.35, and a higher D index value, i.e., 3.26, so it is the best acceptor among all others. HDI and EDI are the terms for hole and electron delocalization index, and both values are positive for all designing molecules. HDI and EDI are the measure of hole and electron density. All molecules have higher HDI values than EDI because they have more hole density, resulting in a higher chance of accepting electrons. HDI values for HNM and HNM1−HNM8 are 5.08, 3.57, 0.33, 3.53, 3.46, 7.31, 6.63, 3.49, and 3.18, respectively. EDI values for HNM and HNM1-HNM8 are 3.11, 3.11, 0.31, 3.00, 2.92, 3.35, 4.96, 2.67, and 2.75, respectively. H_CT measures the degree to which these holes are transmitted when connected to a polymer donor. HNM2 has a higher H_CT value, i.e. 9.22, indicating the best hole transfer among all designed molecules. The integral of hole and electron is defined as the quantitative amount of hole and electron density moved during the charge transfer. Both integral hole and integral electron values are equal to each other, indicating that smooth charge (hole and electron) transfer occurred throughout the system without losing or gaining. Integral transition density helps in the computation of the system's overall charge shift, and its values for HNM and HNM1−HNM8 acceptors are given in Table 11.

3.17. Charge Transfer Analysis. Charge transfer study was performed on the developed molecules (HNM1−HNM8) to verify the enhanced optoelectronic properties. The results indicate that the PTB7-Th polymer was associated with the molecules. Given that the HNM2 molecule has appropriate

https://doi.org/10.1021/acsomega.4c07436
ACS Omega 2024, 9, 44668−44688

Table 11. Calculated EDD Parameters for the Synthetic Reference HNM and Designed HNM1−HNM8 Molecules Based HNM Reference and HNM1−HNM8 Acceptors

molecules	HDI (eV)	EDI (eV)	t index (eV)	H index (eV)	D index(eV)	$H_{\_CT}$ (eV)	Integral hole (HF)	Integral electron (HF)	Integral TD (HF)
HNM	5.08	3.11	−2.48	10.20	0.12	2.61	0.77	0.77	−0.00022
HNM1	3.57	3.11	−1.40	7.17	1.09	2.49	0.85	0.85	0.00485
HNM2	0.33	0.31	−5.96	10.35	3.26	9.22	0.08	0.08	0.00014
HNM3	3.53	3.00	−1.91	6.99	0.67	2.59	0.77	0.77	−0.00075
HNM4	3.46	2.92	−1.00	7.21	1.37	2.37	0.81	0.81	0.00336
HNM5	7.13	3.35	−0.75	6.97	1.87	2.63	0.66	0.66	0.00071
HNM6	6.63	4.96	−1.90	4.95	0.24	2.15	0.80	0.80	0.00086
HNM7	3.49	2.67	−2.69	8.99	0.08	2.77	0.78	0.78	0.00116
HNM8	3.18	2.75	−0.87	8.76	1.52	2.39	0.85	0.85	−0.00095

electron RE values as well as the lowest V_{OC}, E_b, and E_g values, it is advised to use it for charge transfer research, followed by the production of the complex (HNM2-PTB7-Th). The complex (HNM2:PTB7-Th) is shown in Figure 15 in its optimal form following optimization at the theoretical level of M062X/6-31G(d,p). The FMO research in Figure 15 is indicative of the HNM2:PTB7-Th complex investigation at the M062X/6-31G(d,p) level. According to the FMO analysis, the LUMO is located in the end-capped A2 acceptor of the HNM2 molecule, whereas within the PTB7-Th donor polymer, the HOMO component is occupied. The density transition from a PTB7-Th donor polymer to an HNM2 acceptor molecule is confirmed by the charge transfer events. The developed compounds (HNM1−HNM8), and more especially HNM2, should be used in commercial solar cell applications for better photovoltaic character according to the charge transfer study.

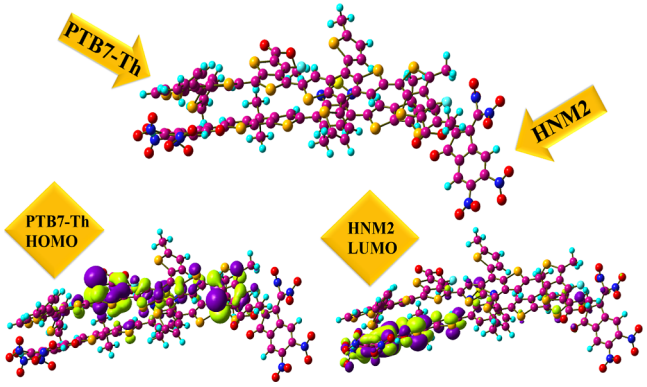

Figure 15. Optimized combination of PTB7-Th:HNM2 (upright) along with FMO distribution patterns (below).

The orbitals of the donor and acceptor that are involved in the charge transfer process are given in Table 12 below. Information that receives charge density is found in the details of the acceptor NBO (antibonding orbitals), while elements that indicate charge density are found in the donor NBO (bonded orbitals). The energy expressed in terms of E2 kcal/mol is needed for this charge transfer mechanism at the donor−acceptor interaction. This transition requires 0.20 kcal/mol of energy. As a result, the C−C bond (C_{108}−C_{113}) provides electron density to antibonding orbitals of the HNM2 acceptor C−N bond (C_{74}−N_{26}) in the bonding orbital of PTB7-Th (donor). By using 0.11 kcal/mol of energy, the C−C bond (C_{114}−C_{125}) of the PTB7-Th (donor) provides electron density to (N_{26}−Se_{27}) of the HNM2 acceptor. This shift, which needs 0.86 kcal/mol of energy, happens when electron density is transferred from the LP (S_{116}) in the bonding orbital of the PTB7-Th (donor) to the antibonding orbitals of the C−H bond in the HNM2 acceptor. When 4.53 kcal/mol of energy is transferred from the donor molecule (PTB7-Th) to the antibonding orbital (C_{81}−O_{86}) via LP (O_{152}), a similar effect is observed.

Moreover, an efficient interfacial charge transfer mechanism is made possible by the donor molecule's hydrogen and carbon atoms being relatively close to the acceptor molecule's sulfur, selenium, and carbon atoms. It can be hypothetically computed that the transfer of charge occurs at the donor−acceptor interface in this way. Because of this, the listed donor and acceptor components are noticeably closer together, and there is a greater chance of charge transfer from those locations in the molecules. Consequently, these elements play a critical role in determining the donor−acceptor interaction's charge transfer mechanism.

4. CONCLUSIONS

In conclusion, a series of eight novel nonfused BSe-based A2-D-A1-D-A2-type NAFs (HNM1−HNM8) were designed by altering the end-capped acceptor (A2) to methodically investigate how the NFR with BSe core affects the optical, optoelectronic, and photovoltaic properties. To examine each of these properties, we employed various calculations using the M062X/6-31G(d,p) level of DFT. Out of all of these planned A2-D-A1-D-A2 symmetric series (HNM1−HNM8), the BSe-based HNM2 demonstrated a significantly enhanced optical absorption of 647.74 nm, whereas the reference HNM molecule displayed an absorption of 631.80 nm using dichloromethane as the solvent. This suggests that HNM2 could be more effective in capturing solar energy, which is crucial for enhancing the light absorption phenomenon and improving the performance of solar cell devices. Moreover, all other developed HNM1, HNM4−HNM5, and HNM7−HNM8 molecules also exhibited better optical capabilities than the reference HNM, whereas the HNM3 (619.92 nm) and HNM6 (610.31 nm) NFA molecules in dichloromethane presented a very close relation in contrast to the reference HNM. Moreover, the designed series also presented a much lower E_g of 3.41 eV (HNM2) than the reference HNM molecule, which shows an E_g of 3.69 eV. This is because of exhibiting substantial conjugation, which revealed the hidden potential of side-chain acceptor units to accept electrons. Similarly, calculated E_x 1.91 eV (HNM2) and E_b parameters are also much lower than those of the reference HNM, ensuring an efficient molecular modeling approach. Furthermore, due to the better energy-level alignment of the designed NFAs (HNM1−HNM8) with polymer donor PTB7-Th, a

https://doi.org/10.1021/acsomega.4c07436
ACS Omega 2024, 9, 44668−44688

Table 12. Estimated Energies from the Acceptor HNM2 to the Donor PTB7-Th Polymer Required for Efficient Charge Transfer Process

donor NBO	acceptor NBO	E_2 kcal/mol
$BD_{(2)}$ C_{108}–C_{113}	$BD_{(2)}^*$ C_{22}–C_{23}	0.52
$BD_{(2)}$ C_{108}–C_{113}	$BD_{(2)}^*$ C_{24}–N_{26}	0.20
$BD_{(2)}$ C_{108}–C_{113}	$BD_{(2)}^*$ C_{29}–C_{33}	0.13
$BD_{(2)}$ C_{109}–C_{110}	$BD_{(2)}^*$ C_{22}–C_{23}	0.24
$BD_{(2)}$ C_{111}–C_{112}	$BD_{(2)}^*$ C_{20}–C_{21}	0.25
$BD_{(2)}$ C_{111}–C_{112}	$BD_{(2)}$ C_{22}–C_{23}	0.20
$BD_{(2)}$ C_{114}–C_{125}	$BD_{(2)}^*$ C_{24}–N_{26}	0.67
$BD_{(2)}$ C_{114}–C_{125}	$BD_{(1)}^*$ N_{26}–Se_{27}	0.11
$BD_{(2)}$ C_{115}–C_{126}	$BD_{(1)}^*$ C_{22}–H_{59}	0.21
$BD_{(2)}$ C_{117}–C_{118}	$BD_{(2)}^*$ C_{31}–C_{32}	0.12
$BD_{(2)}$ C_{120}–C_{121}	$BD_{(2)}^*$ C_{16}–C_{17}	0.23
$BD_{(2)}$ C_{120}–C_{121}	$BD_{(2)}^*$ C_{20}–C_{21}	0.64
$BD_{(2)}$ C_{120}–C_{121}	$BD_{(2)}^*$ C_{25}–N_{28}	0.15
$BD_{(2)}$ C_{123}–C_{124}	$BD_{(1)}^*$ Se_{27}–N_{28}	0.33
$BD_{(1)}$ C_{125}–H_{135}	$BD_{(2)}^*$ C_{29}–C_{33}	0.14
$BD_{(1)}$ C_{125}–H_{135}	$BD_{(1)}^*$ C_{33}–H_{60}	0.15
$BD_{(1)}$ C_{126}–H_{136}	$BD_{(1)}^*$ S_{30}–C_{31}	0.13
$BD_{(2)}$ C_{142}–C_{146}	$BD_{(2)}^*$ C_{34}–C_{35}	0.23
$BD_{(2)}$ C_{147}–C_{148}	$BD_{(1)}^*$ C_{34}–S_{37}	0.13
$BD_{(2)}$ C_{147}–C_{148}	$BD_{(2)}^*$ C_{38}–C_{39}	0.11
$BD_{(1)}$ C_{150}–O_{152}	$BD_{(2)}^*$ C_{81}–O_{86}	0.25
$BD_{(1)}$ C_{154}–H_{157}	$BD_{(2)}^*$ C_{44}–C_{82}	0.18
$BD_{(1)}$ C_{155}–H_{158}	$BD_{(2)}^*$ N_{96}–O_{98}	0.13
$BD_{(1)}$ C_{155}–H_{160}	$BD_{(1)}^*$ C_{42}–H_{68}	0.11
$BD_{(2)}$ C_{161}–C_{166}	$BD_{(2)}^*$ C_{2}–C_{6}	0.17
$BD_{(2)}$ C_{161}–C_{166}	$BD_{(2)}^*$ C_{71}–O_{74}	0.85
$BD_{(2)}$ C_{162}–C_{163}	$BD_{(2)}^*$ C_{2}–C_{6}	0.19
$BD_{(2)}$ C_{162}–C_{163}	$BD_{(2)}^*$ C_{7}–C_{11}	0.23
$BD_{(2)}$ C_{164}–C_{165}	$BD_{(2)}^*$ C_{1}–C_{72}	0.96
$BD_{(2)}$ C_{164}–C_{165}	$BD_{(2)}^*$ C_{2}–C_{6}	0.20
$BD_{(2)}$ C_{168}–C_{179}	$BD_{(2)}^*$ C_{7}–C_{11}	0.35
$BD_{(2)}$ C_{168}–C_{179}	$BD_{(1)}^*$ C_{11}–H_{50}	0.05
$BD_{(2)}$ C_{180}–C_{181}	$BD_{(1)}^*$ C_{19}–H_{56}	0.28
$BD_{(1)}$ C_{183}–H_{193}	$BD_{(1)}^*$ N_{75}–O_{80}	0.10
$BD_{(2)}$ C_{196}–C_{200}	$BD_{(2)}^*$ C_{9}–C_{10}	0.13
$BD_{(2)}$ C_{201}–C_{202}	$BD_{(2)}^*$ C_{16}–C_{17}	0.11
$BD_{(2)}$ C_{201}–C_{202}	$BD_{(1)}^*$ C_{19}–H_{57}	0.13
$LP_{(1)}$ S_{116}	$BD_{(1)}^*$ C_{41}–H_{66}	0.86
$LP_{(2)}$ S_{119}	$BD_{(2)}^*$ C_{20}–C_{21}	0.95
$LP_{(2)}$ S_{143}	$BD_{(1)}^*$ C_{41}–H_{66}	1.62
$LP_{(2)}$ S_{149}	$BD_{(1)}^*$ S_{37}–C_{38}	0.23
$LP_{(2)}$ O_{152}	$BD_{(2)}^*$ C_{81}–O_{86}	4.53
$LP_{(1)}$ F_{153}	$BD_{(1)}^*$ C_{83}–N_{96}	0.13
$LP_{(2)}$ S_{169}	$BD_{(2)}^*$ C_{71}–O_{74}	0.24
$LP_{(2)}$ S_{172}	$BD_{(2)}^*$ C_{1}–C_{72}	1.21
$LP_{(1)}$ S_{175}	$BD_{(2)}^*$ C_{3}–C_{69}	0.23
$LP_{(2)}$ S_{182}	$BD_{(1)}^*$ C_{6}–H_{49}	2.85
$LP_{(2)}$ S_{203}	$BD_{(1)}^*$ C_{19}–H_{57}	5.72
$LP_{(3)}$ F_{207}	$BD_{(2)}^*$ C_{25}–N_{28}	0.17

good value of V_{oc} of up to 1.95 V has been calculated for the designed HNM6 molecule, which is comparable with that of the reference HNM molecule. The acceptors HNM1, HNM7, and HNM8 displayed the highest LHE. The EDD analysis of HNM1−HNM8 acceptors highlights how their electronic structure supports efficient light absorption and charge transfer, reinforcing their suitability for use in high-performance solar cell applications. The presence of acceptor moieties with electronegative atoms in designed compounds leads to enhanced charge transfer rates, as demonstrated by the NPA finding. The findings of the RE analysis validate that the developed NFR containing BSe-based A2-D-A1-D-A2 series (HNM1−HNM8) has an electron-accepting nature. Therefore, they demonstrated the potential to absorb more light energy. Due to their improved optical and optoelectronics features, these molecules may hold great promise to advance future solar energy technologies due to their capacity to convert more light into energy. This suggests that these materials could serve as efficient NFA molecules in the future to fabricate cost-effective and high-performance OSCs.

■ ASSOCIATED CONTENT

Data Availability Statement

The data presented in this study are provided in the Supporting Information.

Supporting Information

The Supporting Information is available free of charge at https://pubs.acs.org/doi/10.1021/acsomega.4c07436.

Synthetic reference's and designed molecules' molecular structures and optimized structures of the synthetic reference and designed materials (PDF)

■ AUTHOR INFORMATION

Corresponding Author

Riaz Hussain − *Department of Chemistry, University of Okara, Okara 56300, Pakistan;* orcid.org/0000-0003-4304-0451; Email: riazhussain@uo.edu.pk

Authors

Hira Naz − *Department of Chemistry, University of Okara, Okara 56300, Pakistan*

Muhammad Adnan − *Graduate School of Energy Science and Technology, Chungnam National University, Daejeon 34134, Republic of Korea;* orcid.org/0000-0001-9224-3824

Zobia Irshad − *Graduate School of Energy Science and Technology, Chungnam National University, Daejeon 34134, Republic of Korea;* orcid.org/0000-0002-8130-4414

Hany W. Darwish − *Department of Pharmaceutical Chemistry, College of Pharmacy, King Saud University, Riyadh 11451, Saudi Arabia*

Mahmood Ahmed − *Department of Chemistry, Division of Science and Technology, University of Education, Lahore 54770, Pakistan;* orcid.org/0000-0002-2285-7406

Complete contact information is available at: https://pubs.acs.org/10.1021/acsomega.4c07436

Author Contributions

⊥H.N. and M.A. contributed equally. H.N.: Validation, visualization, formal analysis, and writing—original draft. M.A.: Visualization, validation, conceptualization, methodology, and writing—review and editing. Z.I.: Data curation, formal analysis, and visualization. R.H.: Conceptualization, project administration, data curation, resources, supervision, software, and paper editing. H.W.D.: Methodology, software, validation, and formal analysis. M.A.: Methodology and writing—review and editing.

Notes

The authors declare no competing financial interest.

https://doi.org/10.1021/acsomega.4c07436
ACS Omega 2024, 9, 44668−44688

■ ACKNOWLEDGMENTS

We thank COMSAT University Islamabad, Abbottabad Campus, for providing their state-of-the-art computational facilities. The authors extend their appreciation to the Researchers Supporting Project number (RSPD2024R812), King Saud University, Riyadh, Saudi Arabia, for funding this work.

■ REFERENCES

(1) Ganesamoorthy, R.; Sathiyan, G.; Sakthivel, P. Review: Fullerene based acceptors for efficient bulk heterojunction organic solar cell applications. *Sol. Energy Mater. Sol. Cells* **2017**, *161*, 102−148.
(2) Collavini, S.; Delgado, J. L. Fullerenes: the stars of photovoltaics. *Sustainable Energy Fuels* **2018**, *2* (11), 2480−2493.
(3) Zhou, N.; Guo, X.; Ortiz, R. P.; Harschneck, T.; Manley, E. F.; Lou, S. J.; Hartnett, P. E.; Yu, X.; Horwitz, N. E.; Burrezo, P. M.; et al. Marked consequences of systematic oligothiophene catenation in thieno [3, 4-c] pyrrole-4, 6-dione and bithiopheneimide photovoltaic copolymers. *J. Am. Chem. Soc.* **2015**, *137* (39), 12565−12579.
(4) Speller, E. M.; Clarke, A. J.; Luke, J.; Lee, H. K. H.; Durrant, J. R.; Li, N.; Wang, T.; Wong, H. C.; Kim, J. S.; Tsoi, W. C.; et al. From fullerene acceptors to non-fullerene acceptors: prospects and challenges in the stability of organic solar cells. *J. Mater. Chem. A* **2019**, *7* (41), 23361−23377.
(5) Yuan, J.; Zhang, Y.; Zhou, L.; Zhang, G.; Yip, H.-L.; Lau, T.-K.; Lu, X.; Zhu, C.; Peng, H.; Johnson, P. A.; et al. Single-junction organic solar cell with over 15% efficiency using fused-ring acceptor with electron-deficient core. *Joule* **2019**, *3* (4), 1140−1151.
(6) Cui, Y.; Yao, H.; Zhang, J.; Zhang, T.; Wang, Y.; Hong, L.; Xian, K.; Xu, B.; Zhang, S.; Peng, J.; et al. Over 16% efficiency organic photovoltaic cells enabled by a chlorinated acceptor with increased open-circuit voltages. *Nat. Commun.* **2019**, *10* (1), 2515.
(7) Chai, G.; Zhang, J.; Pan, M.; Wang, Z.; Yu, J.; Liang, J.; Yu, H.; Chen, Y.; Shang, A.; Liu, X.; et al. Deciphering the role of chalcogen-containing heterocycles in nonfullerene acceptors for organic solar cells. *ACS Energy Lett.* **2020**, *5* (11), 3415−3425.
(8) Nian, L.; Kan, Y.; Gao, K.; Zhang, M.; Li, N.; Zhou, G.; Jo, S. B.; Shi, X.; Lin, F.; Rong, Q.; et al. Approaching 16% efficiency in all-small-molecule organic solar cells based on ternary strategy with a highly crystalline acceptor. *Joule* **2020**, *4* (10), 2223−2236.
(9) Mishra, A. Material perceptions and advances in molecular heteroacenes for organic solar cells. *Energy Environ. Sci.* **2020**, *13* (12), 4738−4793.
(10) Wei, Y.; Chen, Z.; Lu, G.; Yu, N.; Li, C.; Gao, J.; Gu, X.; Hao, X.; Lu, G.; Tang, Z.; et al. Binary organic solar cells breaking 19% via manipulating the vertical component distribution. *Adv. Mater.* **2022**, *34* (33), 2204718.
(11) Zhang, G.; Zhao, J.; Chow, P. C.; Jiang, K.; Zhang, J.; Zhu, Z.; Zhang, J.; Huang, F.; Yan, H. Nonfullerene acceptor molecules for bulk heterojunction organic solar cells. *Chem. Rev.* **2018**, *118* (7), 3447−3507.
(12) Mishra, A.; Sharma, G. D. Harnessing the Structure-Performance Relationships in Designing Non-Fused Ring Acceptors for Organic Solar Cells. *Angew. Chem., Int. Ed.* **2023**, *62* (21), No. e202219245.
(13) Wang, X.; Lu, H.; Liu, Y.; Zhang, A.; Yu, N.; Wang, H.; Li, S.; Zhou, Y.; Xu, X.; Tang, Z.; et al. Simple Nonfused Ring Electron Acceptors with 3D Network Packing Structure Boosting the Efficiency of Organic Solar Cells to 15.44%. *Adv. Energy Mater.* **2021**, *11* (45), 2102591.
(14) Cui, T.; Zhang, Y.; Fei, X.; Ding, Y.-T.; Zhang, Z.-Q.; Wang, T.; Sun, C. L.; Zhu, Q.; Xin, J.; Seibt, S.; et al. Efficient and Stable Nonfused Ring Small Molecule Acceptors Powered by an Electron Donating Unit for Organic Solar Cells. *ACS Appl. Energy Mater.* **2022**, *5* (11), 13861−13870.
(15) Ma, L.; Zhang, S.; Zhu, J.; Wang, J.; Ren, J.; Zhang, J.; Hou, J. Completely non-fused electron acceptor with 3D-interpenetrated crystalline structure enables efficient and stable organic solar cell. *Nat. Commun.* **2021**, *12* (1), 5093.
(16) Fan, B.; Lin, F.; Wu, X.; Zhu, Z.; Jen, A. K.-Y. Selenium-containing organic photovoltaic materials. *Acc. Chem. Res.* **2021**, *54* (20), 3906−3916.
(17) Zhang, Z.; Li, Y.; Cai, G.; Zhang, Y.; Lu, X.; Lin, Y. Selenium heterocyclic electron acceptor with small urbach energy for as-cast high-performance organic solar cells. *J. Am. Chem. Soc.* **2020**, *142* (44), 18741−18745.
(18) Song, Y.; Zhong, Z.; Li, L.; Liu, X.; Huang, J.; Wu, H.; Li, M.; Lu, Z.; Yu, J.; Hai, J. Fused-heterocycle engineering on asymmetric non-fullerene acceptors enables organic solar cells approaching 29 mA/cm2 short-circuit current density. *Chem. Eng. J.* **2022**, *430*, 132830.
(19) Zhang, J.; Luo, S.; Zhao, H.; Xu, X.; Zou, X.; Shang, A.; Liang, J.; Bai, F.; Chen, Y.; Wong, K. S.; et al. Precise Control of Selenium Functionalization in Non-Fullerene Acceptors Enabling High-Efficiency Organic Solar Cells. *Angew. Chem.* **2022**, *134* (46), No. e202206930.
(20) Casanova, N.; Shankar S, S.; Gómez-Escalonilla, M. J.; de la Cruz, P.; Singhal, R.; Sharma, G. D.; Langa, F. Improved Efficiency in Organic Solar Cells Based on A2-D-A1-D-A2 Nonfullerene Acceptors with a Benzoselenadiazole Core Induced by Higher Dipole Moment and Dielectric Constant. *ACS Appl. Energy Mater.* **2023**, *6* (23), 12052−12063.
(21) He, C.; Li, Y.; Li, S.; Yu, Z.-P.; Li, Y.; Lu, X.; Shi, M.; Li, C. Z.; Chen, H. Near-infrared electron acceptors with unfused architecture for efficient organic solar cells. *ACS Appl. Mater. Interfaces* **2020**, *12* (14), 16700−16706.
(22) Yuan, L.; Liang, S.; Xiao, C.; Chen, Q.; Li, W. Near-Infrared Nonfullerene Acceptors Based on 4H-Cyclopenta [1, 2-b: 5, 4-b′] dithiophene for Organic Solar Cells and Organic Field-Effect Transistors. *Chem.—Asian J.* **2021**, *16* (24), 4171−4178.
(23) Parr, R. G. Density functional theory. In *Electron Distributions and the Chemical Bond*; Springer, 1982; pp 95−100.
(24) Caricato, M.; Frisch, M. J.; Hiscocks, J.; Frisch, M. J. *Gaussian 09*. IOps; Gaussian Wallingford: CT, USA, 2009.
(25) Dennington, R.; Keith, T. A.; Millam, J. M. *GaussView*, version 6.0 16, Semichem Inc.: Shawnee Mission, KS, 2016.
(26) Civalleri, B.; Zicovich-Wilson, C. M.; Valenzano, L.; Ugliengo, P. B3LYP augmented with an empirical dispersion term (B3LYP-D*) as applied to molecular crystals. *CrystEngComm* **2008**, *10* (4), 405−410.
(27) Adamo, C.; Barone, V. Exchange functionals with improved long-range behavior and adiabatic connection methods without adjustable parameters: The m PW and m PW1PW models. *J. Chem. Phys.* **1998**, *108* (2), 664−675.
(28) Yanai, T.; Tew, D. P.; Handy, N. C. A new hybrid exchange−correlation functional using the Coulomb-attenuating method (CAM-B3LYP). *Chem. Phys. Lett.* **2004**, *393* (1−3), 51−57.
(29) Chai, J.-D.; Head-Gordon, M. Long-range corrected hybrid density functionals with damped atom−atom dispersion corrections. *Phys. Chem. Chem. Phys.* **2008**, *10* (44), 6615−6620.
(30) Wang, Y.; Verma, P.; Zhang, L.; Li, Y.; Liu, Z.; Truhlar, D. G.; He, X. M06-SX screened-exchange density functional for chemistry and solid-state physics. *Proc. Natl. Acad. Sci. U.S.A.* **2020**, *117* (5), 2294−2301.
(31) *OriginLab Corporation*, Version O; OriginLab Corporation, Northampton, MA, USA. 2021; *5*, 1−15.
(32) O'boyle, N. M.; Tenderholt, A. L.; Langner, K. M. Cclib: a library for package-independent computational chemistry algorithms. *J. Comput. Chem.* **2008**, *29* (5), 839−845.
(33) Lu, T.; Chen, F. Multiwfn: A multifunctional wavefunction analyzer. *J. Comput. Chem.* **2012**, *33* (5), 580−592.
(34) Adnan, M.; Irshad, Z.; Lee, J. K. Facile all-dip-coating deposition of highly efficient (CH 3) 3 NPbI 3− x Cl x perovskite materials from aqueous non-halide lead precursor. *RSC Adv.* **2020**, *10* (48), 29010−29017.

https://doi.org/10.1021/acsomega.4c07436
ACS Omega 2024, 9, 44668−44688

(35) Zhao, Y.; Truhlar, D. G. The M06 suite of density functionals for main group thermochemistry, thermochemical kinetics, noncovalent interactions, excited states, and transition elements: two new functionals and systematic testing of four M06-class functionals and 12 other functionals. *Theor. Chem. Acc.* **2008**, *120*, 215−241.
(36) Mahmood, A.; Tang, A.; Wang, X.; Zhou, E. First-principles theoretical designing of planar non-fullerene small molecular acceptors for organic solar cells: manipulation of noncovalent interactions. *Phys. Chem. Chem. Phys.* **2019**, *21* (4), 2128−2139.
(37) Adnan, M.; Lee, J. K. All sequential dip-coating processed perovskite layers from an aqueous lead precursor for high efficiency perovskite solar cells. *Sci. Rep.* **2018**, *8* (1), 2168.
(38) Uzun, K. K.; Sayın, S.; Çevik, U. Electronic structure and photophysical properties of some promising organic molecules for organic solar cells. *J. Mol. Model.* **2023**, *29* (10), 323.
(39) Adnan, M.; Lee, W.; Irshad, Z.; Kim, S.; Yun, S.; Han, H.; Chang, H. S.; Lim, J. Managing Interfacial Defects and Charge-Carriers Dynamics by a Cesium-Doped SnO2 for Air Stable Perovskite Solar Cells. *Small* **2024**, *11*, 2402268.
(40) Palomo, L.; Favereau, L.; Senthilkumar, K.; Stępień, M.; Casado, J.; Ramírez, F. J. Simultaneous detection of circularly polarized luminescence and raman optical activity in an organic molecular lemniscate. *Angew. Chem., Int. Ed.* **2022**, *61* (34), No. e202206976.
(41) Hussain, R.; Adnan, M.; Irshad, Z.; Muhammad, S.; Khan, M. U.; Lim, J. Environmentally compatible 3-dimensional star-shaped donor materials for efficient organic solar cells. *Int. J. Energy Res.* **2022**, *46* (15), 22145−22161.
(42) Mary, Y. S.; Mary, Y. S.; Resmi, K.; Kumar, V. S.; Thomas, R.; Sureshkumar, B. Detailed quantum mechanical, molecular docking, QSAR prediction, photovoltaic light harvesting efficiency analysis of benzil and its halogenated analogues. *Heliyon* **2019**, *5* (11), No. e02825.
(43) Hussain, R.; Adnan, M.; Nawab, S.; Khan, M. U.; Khalid, M.; Irshad, Z.; Ayub, K.; Lim, J. Role of novel carbon-oxygen-bridged Z-shaped non-fullerene acceptors for high efficiency organic solar cells. *Synth. Met.* **2022**, *290*, 117159.
(44) Adnan, M.; Kashif, M.; Irshad, Z.; Hussain, R.; Darwish, H. W.; Lim, J. Advancing optoelectronic characteristics of Diketopyrrolopyrrole-Based molecules as donors for organic and as hole transporting materials for perovskite solar cells. *Spectrochim. Acta, Part A* **2024**, *320*, 124615.
(45) Qundeel, A. M.; Hussain, R.; Shehzad, R. A.; Muhammad, S.; Mustafa, G.; Irshad, Z. Impact of end-capped engineering on the optoelectronic characteristics of pyrene-based non-fullerene acceptors for organic photovoltaics. *Int. J. Quantum Chem.* **2024**, *124* (5), No. e27344.
(46) Kousar, S.; Zafar, F.; Rani, A.; Hussain, R.; Iqbal, J.; Abid, M. A.; Zafar, W. U.; Adnan, M.; Shahi, M. N. In silico end-capped engineering of 4, 4′-dimethyl-[2, 2′-bithiazole] core-based acceptor materials for high-performance organic solar cells. *J. Phys. Org. Chem.* **2023**, *36* (11), No. e4557.
(47) Anand, G.; Sivasubramanian, M.; Manimehan, I.; Ruby, A.; Abinayashri, R.; Asmitha, R. Synthesis, spectroscopic elucidation (FT-IR, FT-Raman, UV−vis), quantum chemical computation (PES, FMO, HOMO−LUMO, MEP, NLO, Hirshfeld) and molecular docking studies on 2-thiophenecarboxamide crystal. *J. Mol. Struct.* **2023**, *1286*, 135586.
(48) Mumit, M. A.; Pal, T. K.; Alam, M. A.; Islam, M. A.-A.-A.-A.; Paul, S.; Sheikh, M. C. DFT studies on vibrational and electronic spectra, HOMO−LUMO, MEP, HOMA, NBO and molecular docking analysis of benzyl-3-N-(2, 4, 5-trimethoxyphenylmethylene) hydrazinecarbodithioate. *J. Mol. Struct.* **2020**, *1220*, 128715.
(49) Safdar, S.; Adnan, M.; Hussain, R.; Yaqoob, J.; Khan, M. U.; Hussain, R.; Irshad, Z.; Alshehri, S. M. Role of 9-phenyl-9H-carbazole based hole transport materials for organic and perovskite photovoltaics. *Synth. Met.* **2023**, *297* (297), 117414.
(50) Shafiq, A.; Adnan, M.; Hussain, R.; Irshad, Z.; Farooq, U.; Muhammad, S. Molecular engineering of anthracene core-based hole-transporting materials for organic and perovskite photovoltaics. *ACS Omega* **2023**, *8* (39), 35937−35955.
(51) Narayan, M. R.; Singh, J. Roles of binding energy and diffusion length of singlet and triplet excitons in organic heterojunction solar cells. *Phys. Status Solidi C* **2012**, *9* (12), 2386−2389.
(52) Ambreen, M.; Adnan, M.; Hussain, R.; Irshad, Z.; Yaqoob, J.; Khan, M. U.; Zafar, F. Elucidating modelling of C≡ N-based carbazole-arylamine hole transporting materials for efficient organic and perovskite solar cells. *J. Phys. Chem. Solids* **2023**, *182*, 111581.
(53) Shntaif, A. H.; Rashi, Z. M.; Al-Sawaff, Z. H.; Kandemirli, F. Quantum chemical calculations on two compounds of proquazone and proquazone type calcites as a calcium sensing receptor (CaSR) inhibitory profiles. *Russ. J. Bioorg. Chem.* **2021**, *47* (3), 777−783.
(54) Irshad, Z.; Lee, W.; Adnan, M.; Choi, Y.; Park, T.; Lim, J. Elucidating Charge Carrier Dynamics in Perovskite-Based Tandem Solar Cells. *Small Methods* **2024**, *8* (2), 2300238.
(55) Clark, A. E.; Sonnenberg, J. L.; Hay, P. J.; Martin, R. L. Density and wave function analysis of actinide complexes: What can fuzzy atom, atoms-in-molecules, Mulliken, Löwdin, and natural population analysis tell us? *J. Chem. Phys.* **2004**, *121* (6), 2563−2570.
(56) Nalçakan, H.; Kurtay, G.; Sarıkavak, K.; Şen, N.; Sevin, F. Computational insights into bis-N, N-dimethylaniline based D-π-A photosensitizers bearing divergent-type of π-linkers for DSSCs. *J. Mol. Graphics Modell.* **2023**, *122*, 108485.

https://doi.org/10.1021/acsomega.4c07436
ACS Omega 2024, 9, 44668−44688